

LIPID BODY FUNCTION AS NON-CLASSICAL CALCIUM STORES IN IMMUNOCYTES

A THESIS SUBMITTED TO THE GRADUATE DIVISION OF THE  
UNIVERSITY OF HAWAI‘I AT MĀNOA IN PARTIAL FULFILLMENT  
OF THE REQUIREMENTS FOR THE DEGREE OF

MASTER OF SCIENCE

IN

MICROBIOLOGY

DECEMBER 2014

By

Nolwenn K. Phan

Thesis Committee:

Helen Turner, Chairperson

Paul Patek

Steven Robinow

Keywords: lipid bodies, calcium, mast cell, inflammation, obesity

## **Acknowledgements**

I would like to extend a special thank you to Dr. Helen Turner, my thesis advisor and mentor. I would have never completed this body of work without her guidance, help, and insight. No words can clearly express just how grateful I am to have joined IST lab.

I'd like to express my gratitude to my committee members, Dr. Paul Patek and Dr. Steven Robinow, for their support and guidance through the process of completing this body of work.

A huge thank you to my wonderful lab members: Lori Shimoda, Dr. Kristina Maatoft-Udsen, Carl Sung, Dr. Eric Umemoto, Noelle Rysavy, Januaría Balajadia, Dr. Mark Speck and all other members of Lab 9, for their support and assistance. I have enjoyed working with all of you and am grateful for all the encouragement and good times we have had.

Last but not least, I would like to thank my family and friends for their endless support over the past two years. These past years were filled with highs and lows but their encouragement and love never ceased.

## **Abstract**

Lipid bodies, found in most eukaryotic cells, are intracellular lipid storage organelles. The role of lipid bodies has been most studied in adipocytes and hepatocytes due to their role in energy storage. Comparatively, little is known of the role they play in immunocytes. Both in adipocytes/hepatocytes and in cells of the immune system, lipid body numbers are dynamically regulated and can accumulate to pathophysiological levels (steatosis). In both locales this steatotic state can be induced by nutrient overload and metabolic stress, and in the latter also under certain conditions of infection. The over-arching goals of this project are (1) to study the composition (lipid and protein) and functional contributions made by lipid bodies in immunocytes, and (2) to assess the impact of altered lipid body numbers upon cellular function. The work presented in this thesis describes three areas of progress towards these goals. First, we developed a microaspiration method for isolating highly purified lipid bodies, allowing for their ex vitro manipulation and study of lipid/protein content using microscopy. This technique was validated using fluorescence microscopy of the neutral lipid dye Oil Red O in microaspirated lipid bodies. Second, we assessed the impact of the accumulation of lipid bodies (steatosis) on transcytoplasmic calcium signaling, a major activation pathway in the model immune cell system studied here. Third, we tested a new hypothesis arising from our work on transcytoplasmic calcium signaling. The apparent ability of lipid bodies to act as long term loci for calcium accumulation, coupled with recent studies showing that lipid bodies may contain mitochondria and endoplasmic reticulum, led us to hypothesize their potential role as bona fide calcium stores. Our data revealed that the lipid body population within mast cells is not homogenous. However, some LB exhibit the ability to sequester calcium and to release it in the manner of a bona fide calcium store. These observations represent a potentially novel role for lipid bodies and indicate the possibility of their contribution to calcium dynamics in immune cells under both physiological and pathophysiological conditions.

## Table of Contents

<b>ACKNOWLEDGEMENTS.....</b>	<b>2</b>
<b>ABSTRACT.....</b>	<b>3</b>
<b>LIST OF TABLES.....</b>	<b>6</b>
<b>LIST OF FIGURES.....</b>	<b>7</b>
<b>CHAPTER 1.....</b>	<b>8</b>
<b>INTRODUCTION.....</b>	<b>8</b>
1.1. METABOLIC SYNDROME.....	8
1.1.1. <i>Definition of the Metabolic Syndrome</i> .....	8
1.1.2. <i>The relationship between the Metabolic Syndrome and obesity</i> .....	8
1.2. INFLAMMATION.....	9
1.2.1. <i>Systemic inflammation and obesity</i> .....	9
1.2.2. <i>Metabolic inflammation and adipocyte dysfunction</i> .....	9
1.3. MAST CELLS: THEIR BIOLOGY AND IMPLICATION IN METABOLIC INFLAMMATION.....	10
1.4. THE LIPID BODY.....	11
1.4.1. <i>Composition and structure of lipid bodies</i> .....	11
1.4.2. <i>Lipid body biogenesis</i> .....	12
1.4.3. <i>Lipid bodies and inflammatory mediators</i> .....	13
1.5. CALCIUM SIGNALING.....	13
1.6. THESIS GOALS.....	15
<b>CHAPTER 2.....</b>	<b>16</b>
<b>MATERIALS AND METHODS.....</b>	<b>16</b>
2.1. CELL CULTURE.....	16
2.2. CHEMICALS, REAGENTS AND STIMULATIONS.....	16
2.3. OIL RED O PREPARATION AND STAINING.....	16
2.4. CELL LYSIS.....	16
2.5. PROTEIN DETERMINATION ASSAY.....	17
2.6. LIPID BODY STAINING.....	17
2.7. RBL-2H3 CO-STAINING.....	17
2.8. IMAGING.....	17
<b>CHAPTER 3.....</b>	<b>19</b>
<b>AIM I. DEVELOPMENT OF METHODOLOGY FOR ISOLATION OF HIGHLY PURIFIED LIPID</b>	
<b>BODIES.....</b>	<b>19</b>
3.1. INTRODUCTION AND GOALS.....	19
3.1.1. <i>Lipid body purification: the state of the art</i> .....	19
3.1.2. <i>Approach</i> .....	20

3.2. RESULTS.....	21
3.2.1. <i>Microaspiration approach</i> .....	21
3.2.2. <i>Feasibility</i> .....	24
3.2.3. <i>Purity of samples and confirmation of Oil Red O staining</i> .....	26
3.3. DISCUSSION.....	28
3.3.1. <i>Outcome of microaspiration - feasibility</i> .....	28
3.3.2. <i>Alternate approaches</i> .....	29
<b>CHAPTER 4.....</b>	<b>31</b>
<b>AIM II. ASSESSMENT OF THE IMPACT LIPID BODY ACCUMULATION HAS ON</b>	
<b>TRANSCYTOPLASMIC CALCIUM SIGNALING IN MAST CELLS.....</b>	<b>31</b>
4.1. INTRODUCTION AND GOALS.....	31
4.2 RESULTS.....	31
4.2.1. <i>ORO and Fluo-4 dye co-location in RBL-2H3</i> .....	31
4.2.2. <i>Further high-resolution analysis of possible calcium sequestration in lipid bodies</i> .....	34
4.3 DISCUSSION.....	44
<b>CHAPTER 5.....</b>	<b>46</b>
<b>AIM III. IS A LIPID BODY A <i>BONA FIDE</i> CALCIUM STORE ?.....</b>	<b>46</b>
5.1 INTRODUCTION AND GOALS.....	46
5.1.1. <i>Intracellular calcium storing organelles</i> .....	46
5.1.2. <i>Calcium store stimulation</i> .....	46
5.2 RESULTS.....	47
5.2.1. <i>Mast cell lipid bodies display altered calcium levels during whole cell stimulation</i> .....	47
5.2.2. <i>Assessment of isolated mast cell lipid bodies for dynamic calcium storage</i> .....	49
5.3 DISCUSSION.....	51
<b>CHAPTER 6.....</b>	<b>56</b>
<b>DISCUSSION.....</b>	<b>56</b>
<b>BIBLIOGRAPHY.....</b>	<b>59</b>

## **List of Tables**

<b>Title</b>	<b>Page</b>
Table 3.1. Microaspiration parameters and scenarios explored	22
Table 3.2. Considerations concerning feasibility of lipid body microaspiration for proteomics	25

## List of Figures

Title	Page
Figure 1.1. Composition of lipid droplet	11
Figure 1.2. Lipid body biogenesis models	12
Figure 1.3. Mast cell lipid droplet	13
Figure 3.1. Schematic of microaspiration process depicting steps taken to design technique.	21
Figure 3.2. Microinjection needle containing aspirated lipid body.	23
Figure 3.3. Graphs determining amount of lipid body protein per RBL-2H3	26
Figure 3.4. Images depicting live, whole cell Oil Red O staining	27
Figure 3.5. Aspirated Oil Red O-positive lipid bodies	28
Figure 4.1. Live-cell imaging of RBL-2H3 co-stained with Oil Red O and Fluo-4	32
Figure 4.2. Analysis of calcium signaling in ORO <sup>+</sup> and ORO <sup>-</sup> RBL-2H3	33
Figure 4.3. Time series of an RBL-2H3 co-stained with Fluo-4 (488nm) and ORO (568nm)	34
Figure 4.4. ORO and Fluo-4 co-stained RBL-2H3	35
Figure 4.5. Intensity surface plots of RBL-2H3 cell	36
Figure 4.6. Lipid body annotations	37
Figure 4.7. Tiled views of lipid body z-stacks	38
Figure 4.8. Example of lipid body regions of interest	39
Figure 4.9. Fluorescence intensity of ORO and Fluo-4 in lipid body z-stacks	40
Figure 4.10. Example of Fluo-4 fluorescence intensity comparison	41
Figure 4.11. Comparison of lipid body and cytosolic fluo-4 fluorescence intensities	42
Figure 4.12. Three-dimensional renderings of LB1 through LB5	43
Figure 5.1. Mean Fluo-4 fluorescence intensity of RBL-2H3	48
Figure 5.2. Schematic of calcium stimulation in ex vitro lipid body manipulation	49
Figure 5.3. Images of ex vivo lipid body live-staining.	50
Figure 5.4. Lipid body aspirate adhering to microinjection needle	51
Figure 5.5. Lipid droplet association with other organelles.	52
Figure 5.6. Examples of ORO <sup>+</sup> lipid bodies in association with Fluo-4 <sup>+</sup> structures.	53
Figure 5.7. Ultrastructural imaging of lipid bodies.	54

## **Chapter 1.**

### **Introduction**

#### **1.1. Metabolic Syndrome**

##### **1.1.1. Definition of the Metabolic Syndrome**

The metabolic syndrome, initially named Syndrome X, was first described in 1993 as the outcome of a decrease in insulin-mediated glucose uptake resulting in hyperinsulinemia (1). The increase in insulin production and inability to undergo insulin-mediated glucose uptake became associated with a cluster of changes in people. This cluster of conditions included high blood pressure, coronary heart disease, dyslipidemia, and glucose intolerance, and was eventually recognized as a syndrome.

The metabolic syndrome is now identified as a condition which increases the risk of cardiovascular disease and type 2 diabetes in all individuals. Currently five factors are used to determine whether an individual is suffering from the metabolic syndrome: elevated waist circumference, hypertriglyceridemia (elevated triglyceride levels), hypoalphalipoproteinemia (low high-density lipoprotein (HDL) levels), hypertension (high blood pressure), and hyperglycemia (elevated blood glucose levels) (2-4). A consensus on how to diagnose the metabolic syndrome is yet to be reached and currently two methods are followed. Individuals presenting with an elevated waist circumference and two other symptoms or individuals presenting with any three of the five risk factors are considered to have the metabolic syndrome (3, 5).

##### **1.1.2. The relationship between the Metabolic Syndrome and obesity**

Although originally thought to occur solely as a result of hyperinsulinemia, obesity, more specifically abdominal or visceral obesity, is now considered to be another component of the metabolic syndrome (4, 5). Obesity occurs as a result of a positive energy balance where the imbalance between caloric intake and expenditure results in an accumulation of energy or fat within an individual's body. It is important to note that a positive energy balance can also result from established systemic disorders such as hypothyroidism and insulinoma which both have an effect on energy expenditure. However, the most common form of obesity is the result of what is known as the "nutritional transition", where modernization has driven people to lead lives with increased food consumption and decreased physical activity (4, 6, 7).

In order to assess whether an individual is obese, their body mass index or BMI is measured. Two variables factor into determining an individual's BMI - weight and height. Originally the BMI scale ranged from below 18.5 to 30, with the former corresponding to underweight individuals and the latter representing those considered obese. However the growing obesity epidemic has resulted in an expansion of the scale to include grade 1 obesity ( $30 < 35$ ), grade 2 obesity ( $35 < 40$ ), and grade 3 or severe obesity ( $\geq 40$ ) (8).

Due to the increasing number of obese individuals, obesity has become a worldwide epidemic (6, 7, 9-11). If the rate of obesity prevalence continues to follow the increasing trend, 51% of the United States population will be obese by 2030 with 11% being severely obese (9, 11). This increase in obesity has had a dramatic impact on healthcare costs (6, 7, 10, 11). In the United States alone, obesity-related medical costs doubled from \$78.5 million per year in 1998 to \$147 million in 2008 and have been projected to reach annual costs of up to \$957 million by 2030.

## **1.2. Inflammation**

### **1.2.1. Systemic inflammation and obesity**

Obesity and the metabolic syndrome are associated with a new presentation of inflammation referred to as “metaflammation” for metabolically-triggered inflammation or “parainflammation” representing an inflammatory level between basal and inflammatory states (4). Classic inflammatory responses mount quickly, occurring at or around the site of injury or infection (12). These responses are characterized by four cardinal symptoms: redness, swelling, heat and pain (3). Removal or resolution of the trigger usually results in the termination of the inflammatory response. As the response attenuates, the symptoms subside and the body re-establishes homeostasis. However inflammation observed in the obese state differs greatly from the aforementioned description. Most significant is the low-grade and chronic nature of the inflammatory response which appears to be continuously stimulated (3, 4, 12, 13). Metabolic inflammation also differs from traditional inflammation due to its involvement of multiple organ systems. The systemic inflammation has been shown to affect the liver, kidneys, pancreas, muscles, brain, and adipose tissue (12, 13). The persistent nature of metabolic inflammation results in a positive feedback loop which propagates the inflammatory state leading to system-wide health problems.

### **1.2.2. Metabolic inflammation and adipocyte dysfunction**

Metabolic inflammation has been most studied and observed in adipose tissue. It has been observed that adipose tissue consists not only of adipocytes but immune cells as well. Adipocytes

themselves have also been shown to secrete proteins which control metabolic function through paracrine, autocrine, and endocrine pathways (13, 14). These findings demonstrate the potential of adipose tissue to mount large inflammatory responses.

When the body is faced with a positive energy balance or overnutrition, it must find a way to store excess nutrients. The manner in which the body accomplishes this is by expanding its adipose tissue. First, adipose cells expand in size (hypertrophy) until a threshold is reached, followed by the release of signals to commence the differentiation or recruitment of preadipocytes (hyperplasia) (15). This overexpansion of adipose tissue results in an accumulation of immune cells including macrophages, eosinophils, neutrophils, and mast cells as well as increase in adipocytes. So not only does obesity result in the increase of fat deposits in the body it can also potentially have a direct impact on the level or severity of metabolic inflammation.

### **1.3. Mast cells: their biology and implication in Metabolic Inflammation**

The cell type around which this thesis is centered is the mast cell. Mast cells are pro-inflammatory cells responsible for initiating and maintaining inflammatory responses in tissue. They are found wherever the body interfaces with the environment allowing them to quickly react to an environmental stimulus (16). Mast cells are input-output systems where inputs lead primarily to the output of mediators. Receptor binding, physical activators such as temperature or pressure, and cell-to-cell contact are all inducing signals for mast cell activation. Of the mediators secreted by mast cells, the preformed mediators are most understood. The release of histamine, heparin, serotonin, and proteases from mast cells via secretory granules is a well studied and understood pathway. However much less studied and understood is the release of the *de novo* synthesized lipid mediators, prostaglandins and leukotrienes.

Mast cells are traditionally associated with allergic responses due to their release of mediators when stimulated with IgE. However, recent studies have demonstrated their involvement in other pathologies. The role of mast cells in metabolic inflammation is a relatively recent discovery (17, 18). Mast cell knockout mice gained less weight, exhibited improved glucose tolerance, and reduced inflammation in adipose tissue relative to their wild-type controls (18). These findings indicate mast cell involvement in obesity-related pathologies. Although the definitive role of mast cells in metabolic inflammation is still unclear due to the numerous inflammatory cells associated with adipose tissue, they do seem to be a significant factor of the inflammatory process.

Recent work has extended our understanding of mast cell behavior under conditions of metabolic dysregulation. Studies have identified the presence of insulin receptors on mast cells (19), however the role of this hormone remained enigmatic. Greineisen et al. demonstrated that insulin acts as a mast cell regulator, targeting the expansion of a poorly understood organelle, the lipid body (LB), in this cell type (20). Since mast cell LB are reservoirs of lipid-derived pro-inflammatory mediators, this is the first functional linkage between mast cell function and insulin. Since insulin levels are systemically and chronically altered in various metabolic diseases, these findings suggest that the association between insulin, mast cells, and the LB signaling system merits further study.

## 1.4. The Lipid Body

### 1.4.1. Composition and structure of lipid bodies

Lipid bodies, also known as lipid droplets, fat bodies, liposomes or adiposomes, are ubiquitous organelles and have been found in both prokaryotes and eukaryotes (21-24). Having been identified in a variety of organisms, LB are most appreciated for their role as intracellular lipid storage units and have been most characterized in the adipocyte and macrophage foam cells (25). LB are relatively simple structures consisting of a neutral lipid core and a unilamellar phospholipid outer layer (21) (Figure 1.1). The core consists of triacylglycerols and sterol esters while the outer layer is made primarily of phosphatidylcholine. Embedded within this outer layer are PAT (perilipin, ADRP or adipose differentiation-related protein, TIP47 or tail-interacting protein of 47 kDa) family proteins which have been shown to play a role in the regulate lipid storage metabolism (26-29).

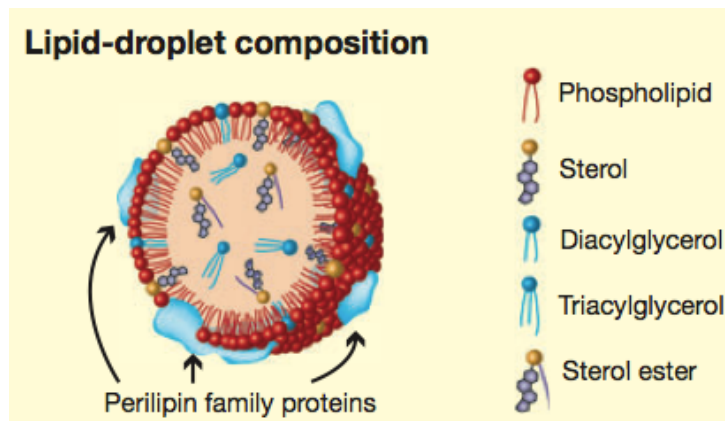


**Figure 1.1. Composition of lipid droplet.** A unilamellar phospholipid layer containing various perilipin family proteins, sterols and diacylglycerols surrounds a neutral lipid core made up of triacylglycerols and sterol esters. From Guo et al. *J Cell Sci.* (2009) 122: 749-752.

Historically, LB have been understudied and thought to serve little function aside from storing high-energy lipids. However, recent studies have ignited interest in their potential role as sites of

inflammatory mediator production (25). These findings would correlate with the inflammatory nature of adipose tissue during obesity.

### 1.4.2. Lipid body biogenesis

Eukaryotic LB are thought to originate from the endoplasmic reticulum (ER) however their biogenesis is not yet fully understood. Electron and fluorescent microscopy have depicted a close relation between LB and the ER (30, 31), however how and why LB dissociate from the ER is still uncertain. Several biogenesis models have been proposed, each depicting some form of ER membrane involvement in the formation of the LB phospholipid outer layer (Figure 1.2). Of the theorized models, ER-budding is most commonly agreed upon. Lipids are synthesized via the neutral lipid synthesizing enzymes (NLSE) and accumulate between the luminal and cytoplasmic leaflets of the ER (21, 31, 32). This accumulation of lipid forms a domain which eventually buds off creating the freestanding LB organelle.

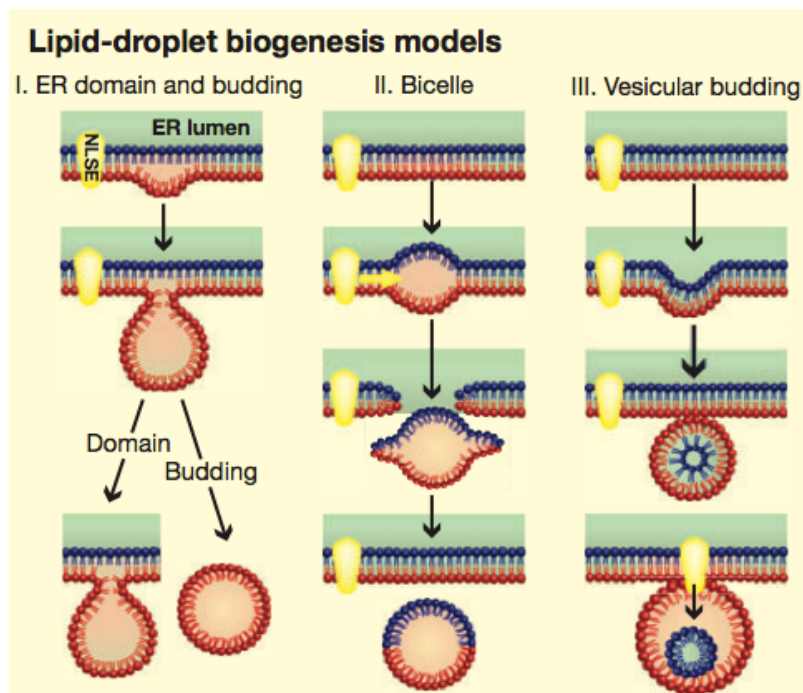


**Figure 3.2. Lipid body biogenesis models.** In Models I and II neutral lipid synthesizing enzymes produce lipid which accumulates between the leaflets of the ER. Lipid bodies are then formed via budding in Model I and excision in Model II. However in vesicular budding (Model III), neutral lipids accumulate into a vesicle bilayer leading to the inclusion of the luminal leaflet of the ER within the lipid body structure. From Guo et al. *J Cell Sci.* (2009) 122: 749-752.

LB expansion is triggered under conditions of metabolic pressure and is very taxing on the cell. Expansion of the LB population requires a cell to synthesize more phosphatidylcholine to replace the phosphatidylcholine loss from the ER.

### 1.4.3. Lipid bodies and inflammatory mediators

LB have been shown to contain the substrates and enzymes required for the synthesis of powerful lipid-derived mediators (25, 33). Experiments using tritiated arachidonic acid and immunogold staining identified the presence of arachidonic acid and cyclooxygenase (COX) in the LB structure of immune cells (32). Mast cell lipid droplets contain two major precursors for arachidonic acid synthesis - triglycerides within the neutral lipid core and phospholipids which form the outer layer of a LB. Given that mast cell LB also contain cyclooxygenase, 5-lipoxygenase, and cytochrome P450, conversion of arachidonic acid into the eicosanoid mediators could potentially be occurring within LB (25). These studies present a possible link between LB and the release of lipid-derived mediators from mast cells. Further study of this link could expand our knowledge of LB function and provide insight into the role LB play in mast cells.

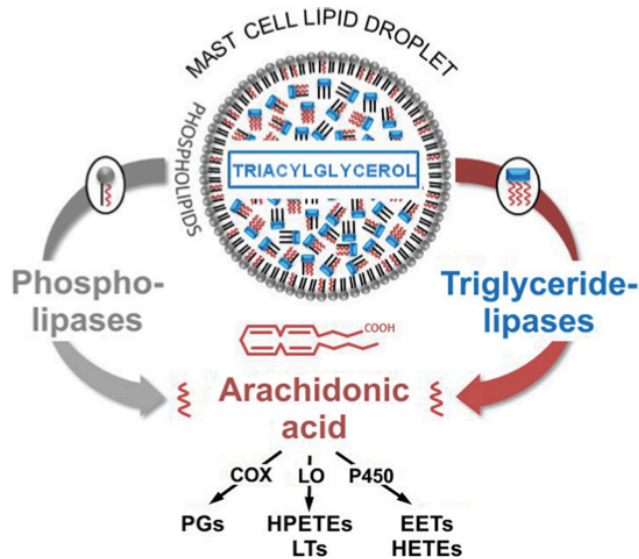


**Figure 1.3. Mast cell lipid droplet.** The triglycerides found in the lipid body neutral core and phospholipid outer layer can be converted into arachidonic acid via triglyceridelipases and phospholipases respectively. The arachidonic acid can then be converted into lipid-derived mediators via cyclooxygenase, 5-lipoxygenase, and cytochrome P450. From Dichlberger et al. *Clin Sci.* (2013) 125(3): 121-130.

## 1.5. Calcium signaling

Along with phosphate, calcium plays a central role in cell signaling. Calcium is a ubiquitous intracellular signaling ion that regulates numerous cellular functions. The effectiveness of calcium in this role is the outcome of a large concentration gradient established across cell membranes. Extracellular concentrations of calcium are in the millimolar (mM) range while intracellular calcium is in the nanomolar (nM) range.

Calcium signaling operates in an ON/OFF fashion and depends on the established gradient (34). ON mechanisms rely on the entry of extracellular calcium into the cell or the release of calcium from internal stores, via calcium channels. The plasma membrane contains several channels, which allow calcium to enter cells. Voltage operated channels are activated by membrane depolarization and are well understood. External calcium can also enter the cell through receptor-operated channels, which respond to the binding of extracellular ligands. Least understood of the plasma membrane channels, are the store-operated channels, which open in response to internal calcium store depletion. In order to access internal calcium stores, the inositol-(1,4,5)-trisphosphate (IP<sub>3</sub>) and ryanodine receptors (RYR) must be triggered. Situated in the endoplasmic reticulum, these channels release calcium from the ER in response to calcium concentration changes within the cytosol. Calcium is rapidly removed from the cytoplasm in order to terminate signaling. The efficacy of termination relies on the OFF mechanisms. SERCA (sarcoplasmic/endoplasmic reticular calcium ATPase) and PMCA (plasma membrane calcium ATPase) pumps push calcium back into the endoplasmic reticulum and extracellular space respectively. These events occur rapidly, allowing the cell to return to a homeostatic state and enabling future signaling to occur.

The ER and mitochondria are heterogeneously spread out within the cytosol allowing for the rapid uptake of calcium. Little is known of the calcium concentrations within these stores. Due to the heterogeneous distribution of calcium-binding proteins within the ER membrane, it is theorized that the calcium distribution within the ER would also be heterogeneous (35). Studies have identified numerous organelles capable of releasing calcium, among them being endosomes, Golgi vesicles, and lysosomes. In order to be considered a calcium store capable of calcium release, the organelle must contain calcium channels and have a favorable calcium gradient in respect to the cytosol.

Release of calcium from internal stores into the cytosol is a universal mechanism for calcium signaling. This action activates a number of pumps and channels in order to quickly compartmentalize or release calcium from the cytosol. Identifying potential intracellular calcium stores could provide more insight into the calcium signaling dynamics of all cells.

Given that LB are thought to originate from the endoplasmic reticulum, they may have the potential to store and release calcium. If LB are capable of storing calcium, this may have implications regarding the calcium signaling dynamics of many cell types both under normal conditions and in those pathologies (e.g. obesity) where LB numbers are greatly expanded.

## **1.6. Thesis goals**

The main goals of this thesis are 1) to study the composition and functional contributions of LB in immunocytes as well as 2) to assess the impact of altered LB numbers on cellular function. Mast cells are major players in adaptive immunity and type IV hypersensitivity. The goals of this project were:

1. To develop a microaspiration method for the isolation of highly purified LB which would allow for their ex vitro manipulation and study of their protein and lipid content.
2. To assess the impact of lipid accumulation on transcytoplasmic calcium signaling within mast cells.
3. To utilize live-cell staining and stimulation experiments to analyze the ability of LB to function as long-term calcium stores.

## **Chapter 2.**

### **Materials and Methods**

#### **2.1. Cell culture**

RBL-2H3 (ATCC<sup>®</sup> CRL-2256<sup>™</sup>) were grown at 37 °C, 5% CO<sub>2</sub>, and 95% humidity in Dulbecco's Modified Eagle's Medium (Mediatech Inc., Herndon, VA) with 10% heat-inactivated Fetal Bovine Serum (Mediatech) and 2mM L-Glutamine.

#### **2.2. Chemicals, reagents and stimulations**

Lipogenesis was induced by incubating RBL-2H3 cells in IFDI for six days 24 hours after seeding. Insulin-FDI (IFDI) consisted of insulin, FBS, dexamethasone and IBMX at 0.01 mg/mL, 10% w/v, 0.25 micromolar and 2.5 micromolar respectively. All analysis was performed on day 7.

#### **2.3. Oil Red O preparation and staining**

Oil Red O powder was dissolved in isopropanol yielding a 3.5% w/v stock solution which was then gently inverted six times before being left to incubate for 25 minutes at room temperature. The solution was then filtered using a 0.2 µm nylon membrane acrodisc syringe filter (Pall Life Sciences, East Hills, NY) and a 20 mL syringe (BD, Franklin Lakes, NJ) to remove excess particulate. Working concentration was obtained via 70:30 stock ORO:distilled water. The solution was inverted gently five times and left to incubate at room temperature for 20 minutes before being filtered with a 0.2 µm nylon membrane acrodisc syringe filter (Pall Life Sciences, East Hills, NY) and a 10 mL syringe (BD, Franklin Lakes, NJ).

#### **2.4. Cell lysis**

Cells were pelleted (2000 g, 2 min) and washed twice in 1 mL PBS at room temperature. Approximately 2x10<sup>6</sup> cells were lysed on ice for 30 min in 300 microliters of high salt lysis buffer (100 mM Hepes pH 7.4, 150 mM NaCl, 80 mM NaF, 20 mM iodoacetamide, 50 mM PMSF (phenyl methyl sulfonyl fluoride), 500 mg/ml aprotinin, 1.0 mg/ml leupeptin and 2.0 mg/ml chymostatin, 1% (w/v) IGEPAL) dissolved in distilled water. Lysates were pelleted (12,000 g, 30 minutes) at 4 °C and protein-containing supernatant was retrieved.

## **2.5. Protein determination assay**

Two BSA protein standards were generated through ten-fold dilutions of BSA solution from 100 mg/mL to 100 ng/mL and 300 mg/mL to 300 ng/mL.

RBL-2H3 protein samples were matched for total protein levels on the basis of a colorimetric protein determination assay, the *DC* Protein Determination Kit™ (BioRad, Hercules, CA) according to the Manufacturer's instructions. Color development was read at 750 nm.

## **2.6. Lipid body staining**

RBL-2H3 (50,000 per cm<sup>2</sup>) were seeded in MatTek coverslip dishes and incubated for 24 hours before receiving insulin treatment (see Methods 2.2). Lipids were aspirated using FemtoTip 0.5 gauge needles and expelled into 10 microliters of PBS on coverslips. Aspirate was fixed onto coverslip overnight using 4% paraformaldehyde. Fixed coverslips were stained with ORO (see Methods 2.3) and mounted onto slide using Crystal Mount and left to rest for at least 24 hours away from light.

## **2.7. RBL-2H3 co-staining**

Cells (50,000 per cm<sup>2</sup>) were seeded in MatTeK coverslip dishes and incubated for 24 hours before receiving insulin treatment (see Methods 2.2). Live cell experiments comprised 30 min staining at 37°C in media with 4 micromolar Fluo-4 and 0.05% ORO from 5% stock in 70:30 EtOH:water. Media was carefully aspirated and cells were washed twice by gently pipetting 1 mL PBS. Dishes were filled with 1 mL DMEM or PBS for imaging.

## **2.8. Imaging.**

Bright field and fluorescence imaging of cells in MatTek dishes (50,000 cells per cm<sup>2</sup>) were performed on a Nikon Ti Eclipse C1 epi-fluorescence and confocal microscopy system, equipped with heated stage. Available laser lines in FITC, TxRed and Cy5 were supplied by a 488nm 10mW solid state laser, a 561nm 10mW diode pump solid state (DPSS) laser and a 638nm 10mW modulated diode laser. Z stack sizes ranged from 3-8 microns depending on the cell being imaged. Each z disc (optical section) ranged from 0.15-1 micron. Pinhole size for all images was 60 microns. Images were analyzed in NIS Elements (Nikon, Melville, NY). Microapplication was accomplished with Eppendorf CellTram Vario system controlled by an Eppendorf micromanipulator (Eppendorf, Hamburg, Germany). Unless otherwise stated images

were acquired through a Plan Apo VC 100X 1.40 oil objective (Nikon). Excitation and emission of dyes used are as follows: ORO, Ex 561 nm/Ex 590/50 nm; Fluo-4, Ex 488 nm/Ex 515/30 nm.

## **Chapter 3.**

### **Aim I. Development of methodology for isolation of highly purified lipid bodies.**

#### **3.1. Introduction and goals**

Our laboratory has previously performed lipidomic analysis of LB isolated using ultracentrifugation. Ultracentrifugation is the accepted protocol for accumulating LB but there are concerns as to the purity of the sample. Future experiments looking at both the lipidome and proteome of pure LB will rely on unambiguous purification if any useful conclusions are to be drawn. The Goal of Aim 1 was therefore to develop a microaspiration methodology that enabled the isolation of uncontaminated LB samples. These samples could then be studied through lipidomic and proteomic analysis to answer pressing questions about the structure and function of the LB in mast cells.

##### **3.1.1. Lipid body purification: the state of the art**

A common method for harvesting LB has been through the use of ultracentrifugation and fractionation (33, 36). Osmotic shock or ultrasonic vibration is used to disrupt cell membranes resulting in the release of intracellular contents. Sonication is then used to homogenize the suspension. Velocity sedimentation through a sucrose gradient allows for the separation of the homogenate components according to size and density. The outcome of the ultracentrifugation process yields highly enriched but impure fractions, each containing organelles of similar size and density (37).

Ultracentrifugation and fractionation are useful methods for harvesting LB to perform a lipidomic analysis. Both techniques are straightforward and have the potential to yield a high number of LB. Since a lipidome includes analysis of only lipids, the production of fractions containing a mixture of protein and lipid poses little threat to the integrity of the generated data set. However, ultracentrifugation and sedimentation both rely on size and density to separate organelles. Therefore, a fraction containing LB may also contain other organelles of similar size and density. Use of an impure fraction for proteomic analysis would generate a data set with an inaccurate representation of the proteins found in LB.

Aware that ultracentrifugation produces impure samples, we investigated other possible methods through which a more homogeneous sample could be acquired. The technique of using fine needles to aspirate lipid droplets from a homogenate mixture of lysed cells has previously been used in adipocytes (38) and presented a new approach for us to achieve highly enriched samples of LB for subsequent analyses.

Samples acquired through the use of microaspiration have the potential to be homogeneous. The combination of microscopy and microinjection needles allows for a highly selective collection process. It is possible to aspirate and collect only LB due to the precision of the microinjection needles. Lipidome and proteome data sets acquired from these pure samples will consequentially be more reliable and accurate.

Although microaspiration could yield a pure product, it is a technically challenging technique which requires the operator to master the aspiration mechanics in order to aspirate single structures. It has yet to be shown whether this method will be useful when aspirating LB averaging 1 micron in size from mast cells. Whether microaspiration is a useful technique for acquiring the large sample sizes needed for a proteome or lipidome has yet to be explored. There are examples in the literature of microaspiration being applied to harvest organelles such as mitochondria (39) and for the harvesting of fat/oil bodies (similar structures to LB) from *Drosophila* and plants. Here we describe the protocol development and feasibility testing of a method for microaspiration of LB from a mammalian cell line, the RBL-2H3.

### **3.1.2. Approach**

The cell line of choice for these studies is the RBL-2H3. This is a rat basophilic leukemia cell line that recapitulates many of the features of a mucosal mast cell (40). This cell line has several other properties in addition to its pro inflammatory phenotype that renders it useful for the proposed project: (1) cells are adherent, (2) cells express high levels of FcεRI antigen receptors, and (3) cells have a small resting population of LB that we can increase dramatically in number using chronic insulin treatment (20).

Microaspiration has been previously used to isolate organelles similar in size to LB; we believe that this method has the potential to produce the homogenous LB sample required for a proteome. Our approach consisted of developing a microaspiration technique for the isolation and extracellular manipulation of LB. RBL-2H3 cells were densely seeded (100,000 cells/mL) in MatTek coverslip dishes and left to incubate at 37 °C, 5% CO<sub>2</sub>, and 95% humidity for a minimum of 24 hours to allow the cells to re-adhere. Cells were stained with Oil Red O (ORO), a neutral lipid dye which accumulates in lipid structures, and incubated for 30 minutes 37 °C. Excess dye

was removed by gently washing the cells twice with 1 mL of PBS before filling the dish with 1 mL of media for imaging. A fluorescence microscope was used to visualize aspiration of the cells. An Eppendorf CellTram Vario system in combination with a TransferMan NK2 micromanipulator was used to perform the aspiration of LB. Eppendorf Femtotips of different bore sizes, 5 and 0.5 microns, were used to pierce through the cell wall and aspirate the intracellular lipids. To preserve the labile and highly oxidizable lipids, aspirated LB were stored at  $-80^{\circ}\text{C}$ .

Our laboratory is equipped with a Nikon Ti Eclipse C1 epi-fluorescence and confocal microscopy system with a heated stage. The microscope contains filter cubes in the FITC (510/560), Texas Red (TxRed) (608/683), Cyanine5 (Cy5) (663/738) and DAPI (435/485) channels. LB were imaged in both bright field and the TxRed channel allowing for the visualization of ORO positive LB. An Eppendorf CellTram Vario system coupled with an Eppendorf NK2 Transferman micromanipulator allowed for the aspiration of lipid.

## 3.2. Results

### 3.2.1. Microaspiration approach

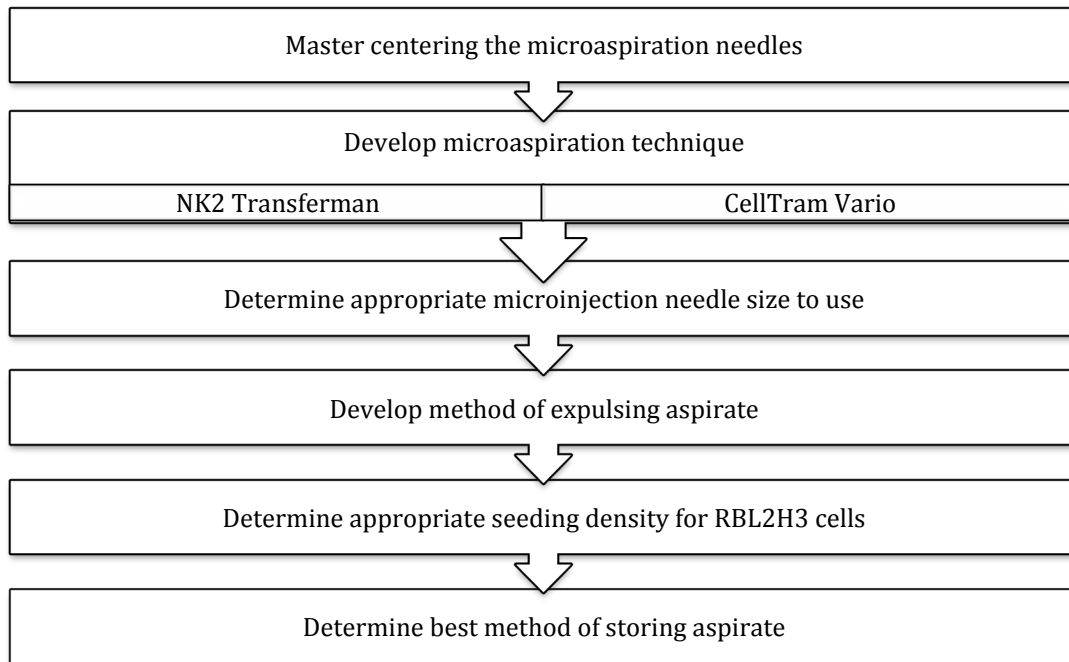


**Figure 3.1. Schematic of microaspiration process depicting steps taken to design technique.**

Microaspiration consists of several steps which had to be optimized in order to collect the LB (Figure 3.1). Centering needles with the use of a micromanipulator was the first step in the process. Working with an accurately centered needle made all subsequent steps less difficult.

Next aspiration through the use of the CellTram Vario was addressed. Once aspiration was possible, we determined which FemtoTip size would be most useful for LB aspiration. We also performed preliminary cell seeding density trials to ensure we would be working with a healthy and heterogeneous cell population. Finally, we considered optimal storage conditions for the aspirate. In order to avoid protein degradation, LB were aspirated in small amounts (contents of five to eight cells) and immediately transferred to 1-mL protease-free Eppendorf microcentrifuge tubes on ice. The tubes contained about 100 microliters of sterile PBS which kept the lipids from drying out. To preserve the integrity and composition of the aspirated lipids, all tubes were stored in a -80°C freezer.

**Table 3. 1. Microaspiration parameters and scenarios explored.** Several parameters were considered during microaspiration development. Table 3.1 includes all considered parameters, details of each parameter, and the outcomes of various troubleshooting scenarios.

Parameter	Details	Outcome
<u>Needle</u>		
5 micron bore	Wide, does not get clogged, aspirates entire cell contents	Lacks precision required to aspirate individual LB
0.5 micron bore	Narrow, clogs easily, highly selective	Clogs upon puncturing cells, requires breaking needle to create larger bore
<u>Needle centering via NK2 Transferman</u>	NK2 Transferman is used for the sequential centering of aspiration needle at 10X, 20X, 40X, 60X and 100X oil-immersion powers	Results in multiple broken needles due to the centers of each objective not being centered on the same point
<u>Cell integrity</u>	RBL-2H3 lift after long periods under the microscope making aspiration difficult	Use of a heated stage at 37°C prolongs cells ability to adhere on converslip dish
<u>Seeding density</u>	Seed dish too densely (> 160,000 cells per cm <sup>2</sup> )	Overcrowded field of view making it difficult to pinpoint lipid bodies
	Seed dish too lightly (< 60,000 cells per cm <sup>2</sup> )	Cells do not grow properly and begin to exhibit abnormal phenotypes

<u>Aspiration via CellTram Vario</u>	CellTram Vario works through vacuum pressure generated by a crank and piston making maintaining the pressure produced difficult	Improper control of aspiration results in the aspiration of too much intracellular contents which can clog needle
<u>Expulsion of aspirate via CellTram Vario</u>	Accumulation of intracellular contents results in needle clogging making it difficult for expulsion	Expulsing aspirate into 10 $\mu$ L PBS creates capillary action aiding in the removal of LB
<u>Purity of aspirate</u>	Larger-bore needles aspirate more than targeted lipid bodies  Small-bore needles clog resulting in an inability to aspirate	Abandoned using 5 micron-bore needle  Breaking a 0.5 micron needle to a 2-3 micron bore made aspiration possible while reducing clogs

Several parameters of microaspiration proved to be challenging (Table 3.1). Aspirating with the larger 5 micron bore needle resulted in aspirating the entire cell while the 0.5 micron needle quickly clogged and unable to aspirate. While breaking the 0.5 micron needle to enlarge the bore is possible, it is challenging to break the needle to a perfect 2-3 micron bore each time. However we determined that a 2 micron diameter needle is optimal for aspirating LB (Figure 3.2).

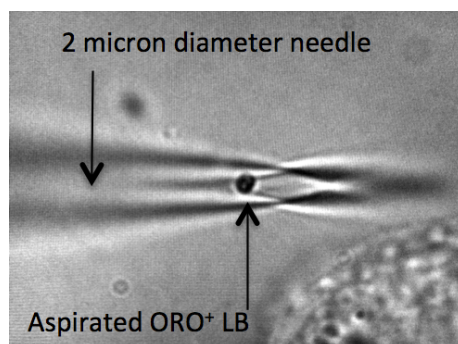


**Figure 3.2. Microinjection needle containing aspirated lipid body.** RBL-2H3 were seeded for 3 days on a MatTek coverslip and stained with ORO as described in Methods. Microaspiration was carried out using an 0.5 micron bore FemtoTip needle, CellTram Vario and a micromanipulator. Image was acquired under 100X phase contract bright field illumination. Cell body is visible at lower right and needle and lipid body are indicated by arrows.

In order to accurately target LB for microaspiration under high-magnification, we needed to center the microinjection needle at each power objective (10X, 20X, 40X, 60X and 100X oil-

immersion), which presented some difficulties during the early stages of technique development. Improper use of the micromanipulator during this process can result in breaking the needle and having to restart the process from the beginning. We observed that seeding density correlates with cell adherence and integrity. We noticed that seeding a dish too sparsely produced cells that lifted quickly during the aspiration process. On the other hand, when we seeded dishes too densely the cells were more adherent to the coverslip dish however, cell crowding made it difficult to target LB. Aspirating in areas of high cell density often resulted in inadvertent clogging of the aspiration needle. We also experienced some challenges aspirating and expelling the aspirate using the vacuum pressure produced by the CellTram Vario. In order to avoid inadvertently aspirating unwanted cellular components, we needed to have the vacuum power in either an on or off setting which required us to maintain a fine control of the Vario.

### **3.2.2. Feasibility**

Several aspects of microaspiration raised concerns regarding the feasibility of the microaspiration technique as a methodology for gathering LB for subsequent experiments. These were (1) the amount of sample needed for analysis, (2) cost, and (3) the time required to complete project (Table 3.2).

**Table 3.2. Considerations concerning feasibility of lipid body microaspiration for proteomics.** Supply cost estimates were determined using needle costs and do not factor in costs of personnel. Number of aspirated cells required and timeframe estimates were calculated using protein assay data (Fig. 3.3) and the protein amounts recommended by Keck MS & Proteomic Resource for MudPIT (Multi-Dimensional Protein Identification Technology) at Yale University.

Parameter	Consideration	
Cost of supplies	Cost per needle	\$25
	Needles used per week	3
	Estimated cost for 6 months	\$1,800
Abundance of LB required (example – for mass spectrometric analysis of proteome)	Amount of protein required for proteome	2-50 micrograms
	Amount of protein per RBL-2H3	0.14 ng
	Amount of LB protein per RBL-2H3	0.043 ng
	Number of aspirated cells required for proteome	46,376 – 1,162,790 cells
Timeframe for aspiration	Cells aspirated per day	75
	Estimated time for project completion	2- 42 years

1. Accumulating enough LB for proteomic analysis was our primary concern. Generating a proteome requires 2-30 micrograms of highly-purified protein (41), with some facilities requesting up to 50 micrograms. Analysis using the BIO-RAD *DC* Protein Assay Kit showed that each RBL-2H3 contains approximately 0.14 ng of protein (Figure 3.3). It was estimated that the LB content of a cell approaches 30%, therefore each cell yields an estimated 0.043 ng of LB protein. Given the low LB protein yield per cell, it became evident that a large number of cells would need to be aspirated in order to obtain an adequate sample for analysis.

2. The cost of funding a microaspiration project are high in both materials and person-hours. We explored reducing costs by re-using needles. Using Trypsin EDTA to remove buildup on the interior and exterior surfaces of the needles allowed for them to be re-used. However it was noticed that the needles became increasingly brittle with each subsequent wash and were only re-usable up to three times.

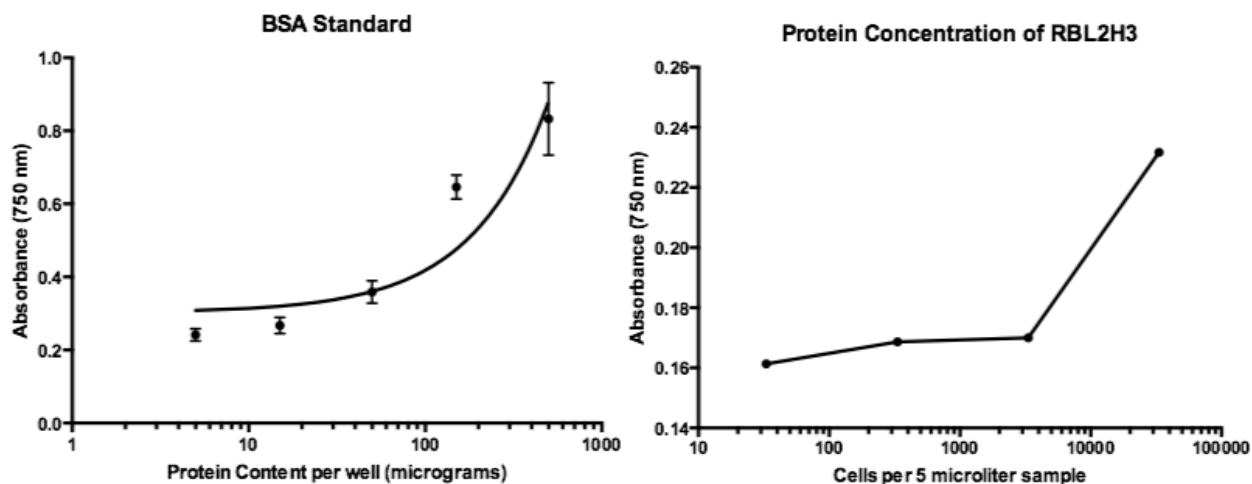


**Figure 3.3. Graphs determining amount of lipid body protein per RBL-2H3.** Cells were harvested and lysed to collect RBL-2H3 protein. The lysate underwent serial logarithmic dilutions from  $2 \times 10^6$  to  $2 \times 10^3$  and a protein standard was generated through dilutions of BSA. All samples were assayed in triplicates

3. Our last concern was the time required to complete the microaspiration project. Given that each RBL-2H3 contains roughly 0.043 ng of LB protein, accumulating a large sample of highly purified lipid would take time (Figure 3.3). The Keck MS & Proteomic Resource recommends a sample amount of 50-200 micrograms for MudPIT proteomic analysis. In order to achieve the recommended minimum of 50 micrograms, 1,162,790 cells would need to be aspirated which could take many years (see Table 3.2).

### 3.2.3. Purity of samples and confirmation of Oil Red O staining

We used ORO staining to determine the purity of the microaspiration samples. ORO is a neutral lipid dye traditionally used to stain fat or lipids in fresh tissue sections and is the standard method for visualizing LB. Pre-staining cells with ORO allowed for a more targeted aspiration of LB. Aspiration must be performed under bright field illumination which allows the cells to be visualized but does not provide any differentiation between intracellular components. Pre-staining the cells made it possible to visualize the lipids under the TxRed channel before being aspirated (Figure 3.4) and made them appear visibly darker under bright field illumination. In this way we can be certain that the organelles being aspirated are indeed LB and not other similarly sized intracellular components. ORO is most commonly used as a histological stain in fixed tissue sections or fixed cells. The use of ORO as a live cell stain required significant optimization, most of which was performed by a prior graduate student in the laboratory.

However, re-optimization was necessary and various doses and time periods of incubation with ORO were tested in live cells, Figure 3.4 shows the results of this optimization. Here, cells were stained for 30 minutes at 37°C in media using 60:40 stock-ORO:water. For optimal results, the 60:40 ORO dye was prepared and filtered just prior to staining.

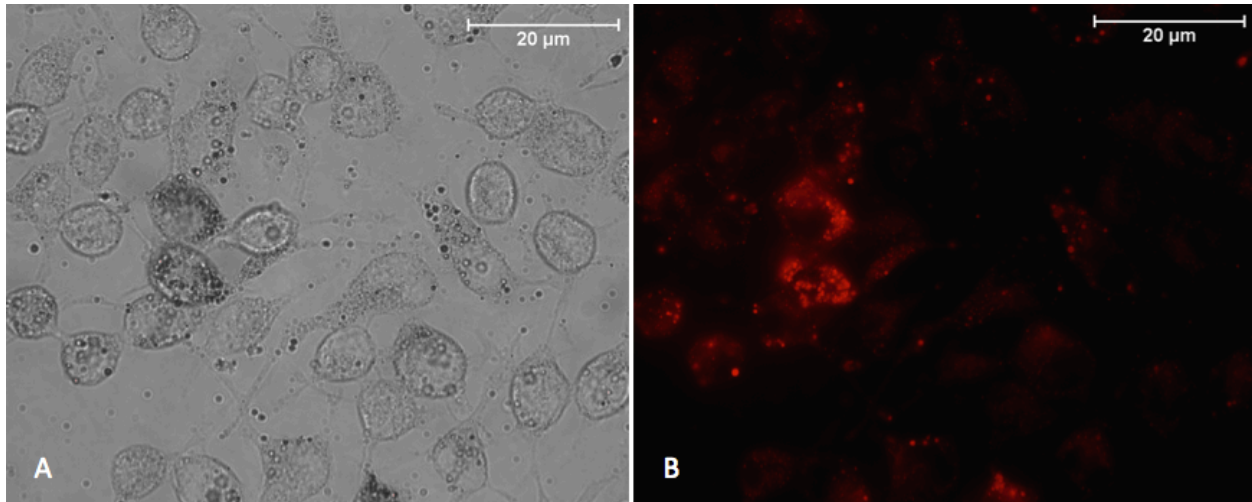


**Figure 3.4. Images depicting live, whole cell Oil Red O staining.** RBL-2H3 were seeded for 2 days on a MatTek coverslip dish and stained with ORO as described in Methods. Images were acquired at 100X power under A) phase contrast bright field illumination and B) Texas Red channel. Lipid bodies are clearly visible in red using fluorescence microscopy and are noticeably darker under phase contrast bright field illumination.

We also assessed the purity of the aspirate through post-staining with ORO. Aspirated lipids were expelled and fixed onto a coverslip followed by 30-minute staining with ORO. Imaging revealed ORO-positive lipids, all of a similar size and shape. Fixing the lipids to a coverslip made it possible to magnify individual lipids to observe their morphology extracellularly (Figure 3.5).

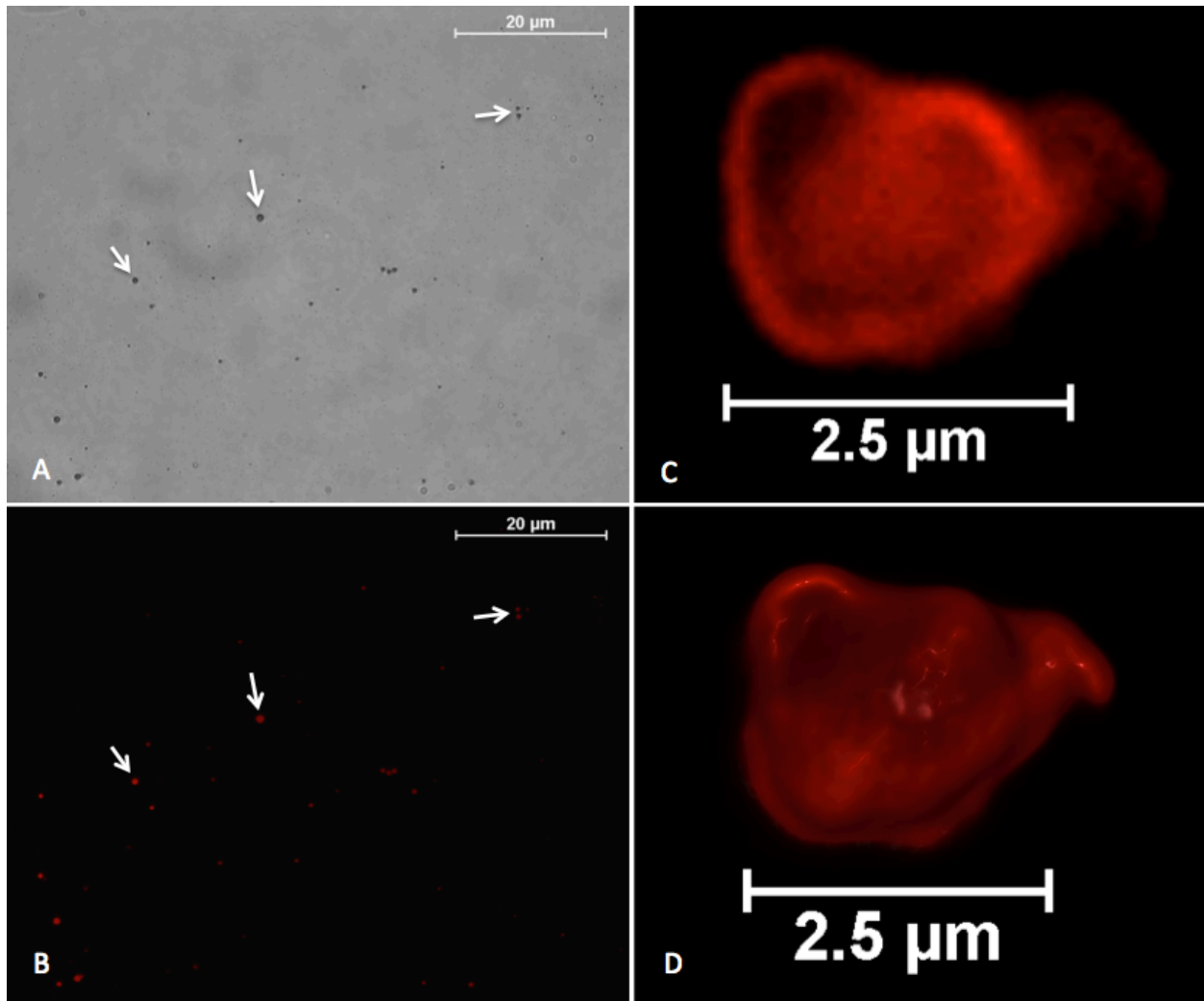


**Figure 3.5. Aspirated Oil Red O-positive lipid bodies.** RBL-2H3 cells were seeded and received insulin treatment as described in Methods. Aspiration of the lipids was performed using a 0.5 micron Femtotip needle, CellTram Vario and a micromanipulator. Aspirate was fixed onto a coverslip as described in Methods. Fixed lipids were stained with ORO and visualized at 100X power under A) phase contrast bright field illumination and B) Texas Red channel. (A,B) Several lipid bodies are indicated with arrows and exhibit positive ORO staining in the Texas Red channel. (C,D) Magnified 100X oil-immersion confocal images of an individual ORO-positive lipid body and a 3-dimensional rendering of the sample lipid.

### 3.3. Discussion

#### 3.3.1. Outcome of microaspiration - feasibility

The goal of this chapter was to develop a technique that would allow for a highly purified LB sample to be obtained. Microaspiration proved to be a promising technique for acquiring a homogenous sample although difficulties were encountered throughout technique development.

Frequent clogging and breaking of the needles made it difficult to accumulate the sample amount required for a proteome. Although two micrograms of protein is potentially enough protein to generate a proteome, the sample collected would need to be of high quality in order to yield good results. A proteome generated with such a small amount of protein could be inaccurate if any unwanted organelles were aspirated into the sample. In order to move forward we would need to collect a large enough sample size to eliminate the risk of any artifacts skewing the data.

The microaspiration technique may be useful if trying to generate a lipidome or proteome of a more abundant organelle. Once we optimized the technique, aspirating LB was relatively straight forward. However, even after insulin stimulation, RBL-2H3 cells do not all produce a large amount of lipid. The biggest challenge became locating lipid-rich cells to aspirate. Given that most proteomic analysis requires a significant amount of high quality protein, we realized that a large number of cells would need to be aspirated. If insulin stimulation resulted in completely steatotic mast cells, the method would be more successful. Not only would the estimated number of aspirated cells decrease but the larger bore needle could be used. A more densely packed cytosol would make the aspiration process less selective while using the larger bore needle would reduce clogging and speed up the collection process.

Although microaspiration did not yield the intended results, it proved to be useful for producing samples of individual LB. The ability to aspirate the lipids and expulse them onto a coverslip with slight pressure dispersed the LB facilitating the imaging process. Co-staining the fixed LB with multiple dyes could yield more insight into their structure and composition. For example staining the LB with an ER tracker dye could potentially allow for the visualization of ER membrane and lamellae within LB.

### **3.3.2. Alternate approaches**

Isolation methods centered around ultracentrifugation and fractionation could be revisited. Stimulating the mast cells with insulin widens the range of LB per cell, resulting in an overall increase of LB production. More LB would not only increase the sample size but also facilitate the fractionation process. LB could then be stained with ORO prior to lysing and sonication, this way the lipid-containing fraction could be identified based on color. However given that this methodology relies on size and density to segregate cellular components, these modifications may not have much of an effect. LB are not homogenous in size. Figure 3.5A and 3.5B demonstrate the wide variety of sizes mast cell LB can achieve. This variation in size could result

in the lipids separating into multiple sucrose layers, making harvesting the appropriate layers difficult.

A combination of high resolution mass spectrometry and nanospray is another potential method of acquiring a mast cell LB proteome. Lipidomes have been acquired using direct infusion mass spectrometry with lipid class-specific scanning. However this method requires additional fragmentation analysis which can hinder the quantification of minor species (42). Even after insulin stimulation, mast cell LB are not produced in overabundance. The ability to generate a proteome using a smaller sample size could make acquiring a mast cell LB proteome more feasible. Nanospray uses low flow rates (nl/min) allowing for the use of smaller samples sizes. These flow rates also consume less sample and reduce background noise, resulting in an enhanced sensitivity of the minor lipid species (42, 43).

We considered using fluorescence-activated cell sorting (FACS) to obtain a LB sample. Theoretically, a large number of RBL-2H3 could be treated with IFDI to induce lipogenesis, and stained with ORO prior to sonication, to fluorescently label the LB. The lysate could then be run through a flow cytometer and the ORO<sup>+</sup> lipids could be sorted resulting in a highly purified lipid sample. However, lipid monolayers and bilayers may not be structurally strong enough to endure the shear forces experienced during flow cytometry. Shear force has been shown to affect fluorescence lifetimes, lipid viscosity, and surface topography of lipid samples (44). Studies have also demonstrated a disruption and increase in lipid membrane fluidity when cells and lipid monolayer models experience shear force resulting in decreased membrane lipid order (45, 46).

We learned that microaspiration of LB is technically challenging however, it can be done. The technique is most suitable for subsequent microscopy and immunohistochemistry analysis rather than techniques that require a large amount of material such as proteomic or lipidomic analysis. However it should be noted that that in Greineisen et al. (in revision, PLOS One), Dr. Turner's laboratory did acquire enough material from aspiration of LB to perform a partial lipidome.

## **Chapter 4.**

### **Aim II. Assessment of the impact lipid body accumulation has on transcytoplasmic calcium signaling in mast cells**

#### **4.1. Introduction and goals**

The presence of such large numbers of lipid structures seems likely to cause dramatic remodeling of the cytoplasm, with subsequent effects on the integrity of cellular signaling pathways. There are few studies directly addressing this issue, but in steatotic hepatocytes and adipocytes there is intriguing evidence of cytoskeletal remodeling (30, 47), altered calcium dynamics, and uncharacterized signaling changes that result in altered functional responses. We set out to look at calcium signaling dynamics in and around LB, as well as the transcytoplasmic calcium signaling in a LB-enriched cytoplasm. More specifically we wanted to observe whether steatotic accumulation of LB has an effect on the progress of transcytoplasmic signals. Steatotic mast cells are phenotypically different than their normal counterparts, creating a need to more fully understand the impact of steatosis on mast cell signaling. While cells that exhibit this steatosis have altered functional phenotypes, the mechanistic links between cytosolic LB accumulation and altered cellular signaling and functional responses have not been explored. The goal of this chapter is to explore the impact of steatosis on calcium signaling dynamics in mast cells.

#### **4.2 Results**

##### **4.2.1. ORO and Fluo-4 dye co-location in RBL-2H3**

The laboratory has established a methodology to simultaneously visualize both calcium responses and LB in live cells. ORO accumulation in discrete LB in live cells was achieved after a period of optimization of staining conditions (see Chapter 2). Figure 4.1A shows that discrete ORO<sup>+</sup> areas of cytoplasm may be visualized in cells co-stained with Fluo-4. At higher magnifications, a single confocal z disc through an ORO<sup>+</sup> area of cytosol shows the distinctive lobed/spherical droplet appearance of LB clusters (16, 20, 31, 32) (Figure 4.1A, inset). ORO-rich areas corresponding to LB may display significant Fluo-4 associated signals (Figure 4.1B & 4.1C) but this is not uniformly the case.

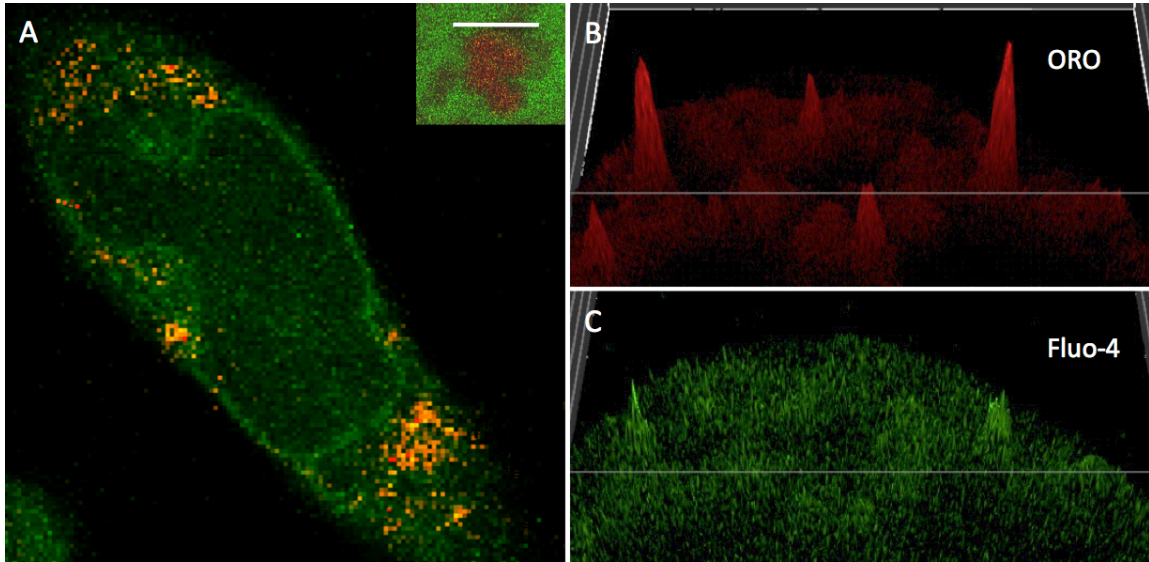


**Figure 4.1. Live-cell Imaging of RBL-2H3 Co-stained with Oil Red O and Fluo-4.** Images depicting positive ORO and Fluo-4 staining of RBL-2H3 A) Z-disc 11 of 21 (main panel) of a cell stained with ORO and Fluo-4, allowing for the visualization of both lipid bodies (red) and calcium (green). Inset panel shows a highly magnified lipid body cluster (scale bar 0.5 microns) stained with ORO and Fluo-4. (B,C) Intensity surface plots showing fluorescence intensity of B) ORO and C) Fluo-4 of a co-stained RBL-2H3. These plots demonstrate that lipid bodies may demonstrate different fluorescence intensities in the red and green fluorescence channels. Panel A acquired by William Greineisen, panels B and C produced by NP.

The laboratory has also developed a whole cell-based, unbiased approach for studying the relationship between LB and calcium flux. Single cell imaging experiments, under conditions of antigen stimulation, were conducted using our live cell ORO protocol. Figures 4.2A and 4.2B show Fluo-4 and ORO localization in a representative cell at rest and after 300 seconds of stimulation respectively. During analysis, the field of view (comprising one 150nm z disc at 100x resolution of a single cell) was divided into several hundred 1 square micron graticule ROI (Figure 4.2B). Each of these graticules was analyzed for its fluorescence profile in both the Texas Red (ORO) and FITC (Fluo-4) channels over time. This approach essentially divides this single cell into 756 distinct calcium assays performed with data collected over 232 time points. Analyses of this type were conducted for 6 cells. Figure 4.2C looks at the overall trend of Fluo-4 response as the mean of ~3000 graticules across 6 cells. Graticules were scored as ORO<sup>lo</sup> (in the lowest 25% of initial ORO fluorescence intensity) or ORO<sup>hi</sup> (in the highest 25% of initial ORO fluorescence intensity), and the mean Fluo-4 intensity of these selected graticules were plotted over time. ORO<sup>lo</sup> cytosol tends to exhibit a classic antigen-induced calcium response. However (Figure 4.2C), across this large data set ORO<sup>hi</sup> areas of cytosol tend to exhibit slowed and

attenuated initial calcium responses in the 0-200s time frame. However, sustained Fluo-4 intensity is significantly higher in ORO<sup>hi</sup> versus ORO<sup>lo</sup> areas of cytosol, leading us to hypothesize that LB may act as long term sinks of calcium similar to the functions postulated for the Golgi apparatus and mitochondria in previous studies (48, 49).

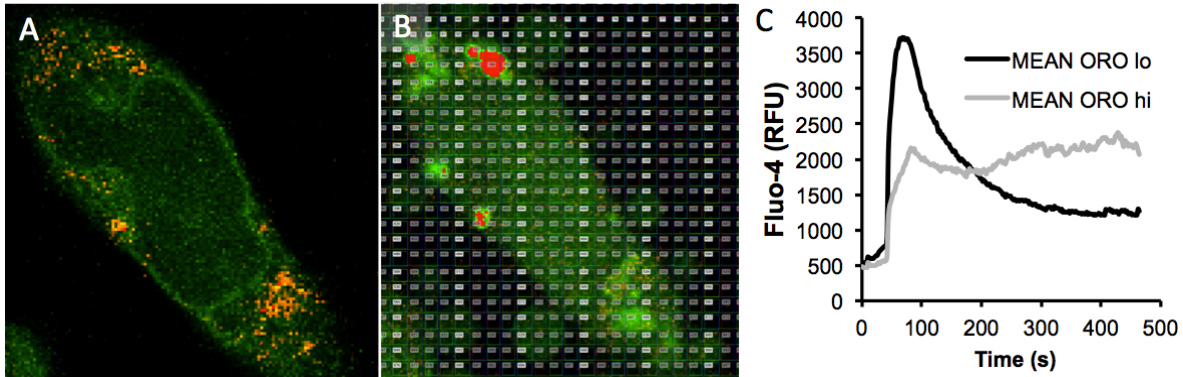


**Figure 4.2. Analysis of Calcium Signaling in ORO<sup>+</sup> and Fluo-4<sup>+</sup> RBL-2H3.** Examples of calcium signaling analysis process (A,B) ORO<sup>+</sup>/Fluo-4<sup>+</sup> RBL-2H3 showing characteristic red (lipid) and green (calcium) fluorescence. B) An example of the graticule ROI placed over a single z-disc of the cell in A. C) Graph showing mean Fluo-4 fluorescence over a time course of 450 seconds after cells received antigen stimulation at 20 seconds. *Black trace.* Averaged signal from graticule ROI within 0- 25<sup>th</sup> percentile ORO fluorescence intensity (ORO<sup>lo</sup>). *Grey trace.* Averaged signal from graticule ROI within 75<sup>th</sup>-100<sup>th</sup> percentile ORO fluorescence intensity (ORO<sup>hi</sup>). Analysis performed prior to my joining the Turner lab by Dr. Mark Speck.

Figure 4.3 shows time course imaging over a period of 400 seconds of the cell in Figure 4.2. At time point zero, the cell exhibits positive ORO and Fluo-4 fluorescence indicating the presence of LB and intracellular calcium respectively. Upon receiving stimulus (20 second time point), Fluo-4 fluorescence intensity rapidly increases resulting in a homogeneous increase in fluorescence by 30 seconds. This increase in fluorescence then declines to sustained levels from 240-400 seconds. While fluorescence within the cytosol decreases, areas of the cell that were initially ORO-positive exhibited an increase in Fluo-4 fluorescence over the 400 second time course. This suggests that calcium levels may remain high in those regions after sarcoplasmic endoplasmic/reticulum calcium-ATPase (SERCA) have depleted the bulk of the cytosol.

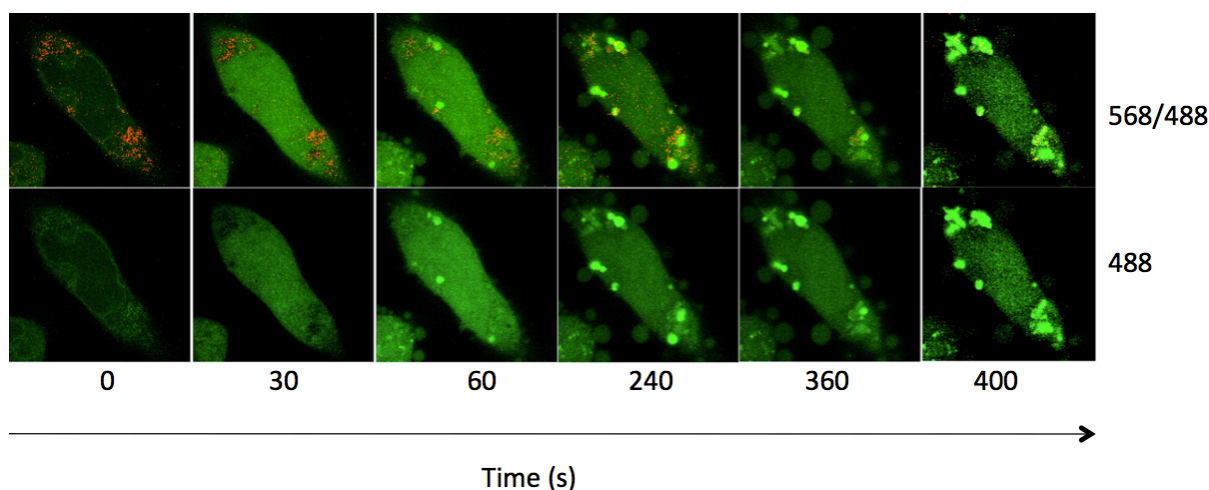


**Figure 4.3. Time series of an RBL-2H3 Co-stained with Fluo-4 (488nm) and ORO (568nm).** Upper panels show both the red (ORO) and green (Fluo-4) channels while only the green channel is shown in the lower panels. The time course is indicated on the bottom in seconds. Antigen stimulus was added at 20 seconds, causing an increase in Fluo-4 intensity. Over the course of 400 seconds several areas of the cell exhibit sustained Fluo-4 fluorescence which initially corresponded to ORO-positive areas. Each panel is one 12 micron z-disc. Imaging performed by William Greineisen prior to my joining the Turner lab.

#### 4.2.2. Further high-resolution analysis of possible calcium sequestration in lipid bodies

Following on from the data presented above, my role in this project started with a high resolution analysis. We selected a cell that very clearly demonstrated positive ORO and Fluo-4 staining which merited further analysis. ORO staining revealed 5 distinct LB, each roughly 1 micrometer in size. The cytosol exhibited Fluo-4 fluorescence in a non-uniform fashion indicating that cytosolic calcium levels are not homogenous throughout (Fig 4.4).

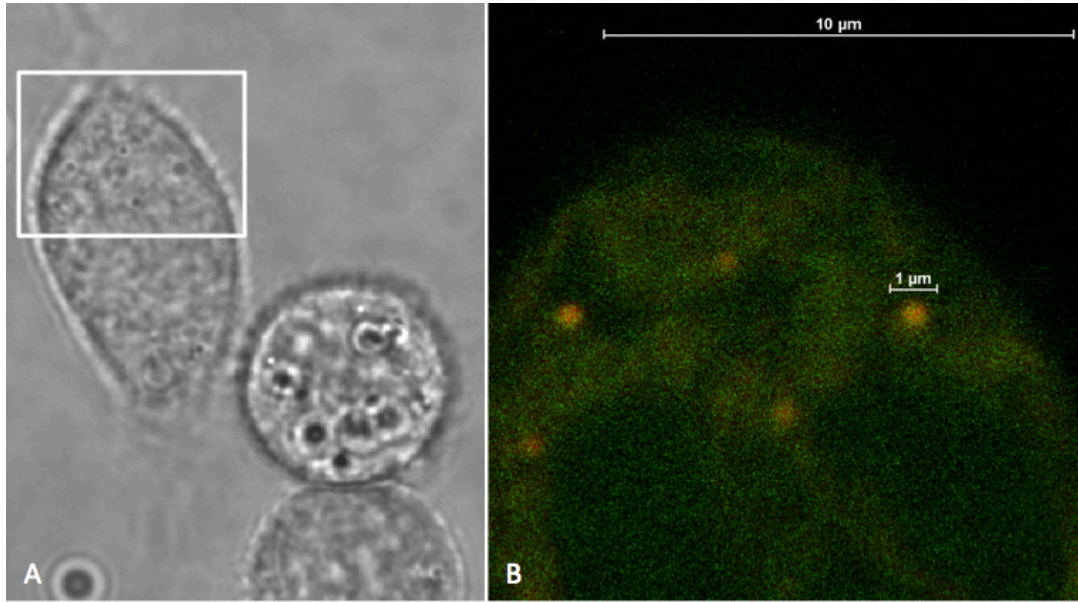


**Figure 4.4. ORO and Fluo-4 co-stained RBL-2H3.** Cells were co-stained with ORO and Fluo-4 dyes and imaged via A) phase contrast bright field illumination and B) confocal microscopy at 100X magnification. A) Three RBL-2H3 cells can be identified with a smaller circular artifact in the lower left-hand corner. A white box is drawn around the portion of the cell which was magnified for confocal imaging. B) The magnified portion of the cell was imaged using the FITC and TxRed lasers. Five lipid bodies (in red) can be viewed throughout the Fluo-4 positive cell body. Intracellular calcium (in green) is heterogeneously dispersed throughout the cytosol. Imaging performed by NP.

Nikon NIS-Elements was used to further analyze the imaging data of the cell. First, we observed ORO and Fluo-4 fluorescence intensities through intensity surface plot (ISP) analysis (Fig. 4.4). Intensity surface plots show the pixel intensity distribution of an image with the height of the z-axis line. An ISP of the red channel showed five distinctive ORO peaks corresponding to the five LB in Figure 4.4. Background ORO staining is also visible however the fluorescence intensity is greatly increased in the LB, indicating an accumulation of the lipid dye within the neutral LB cores. When viewing the ISP in the green channel, two peaks were observed, indicating those areas of the cell had increased Fluo-4 fluorescence intensities relative to the cytosol. Interestingly enough, these peaks were in the same location as two of the ORO intense peaks. This co-location of ORO and Fluo-4 peaks suggested that there may be an accumulation of calcium within lipid-rich regions of the cell.

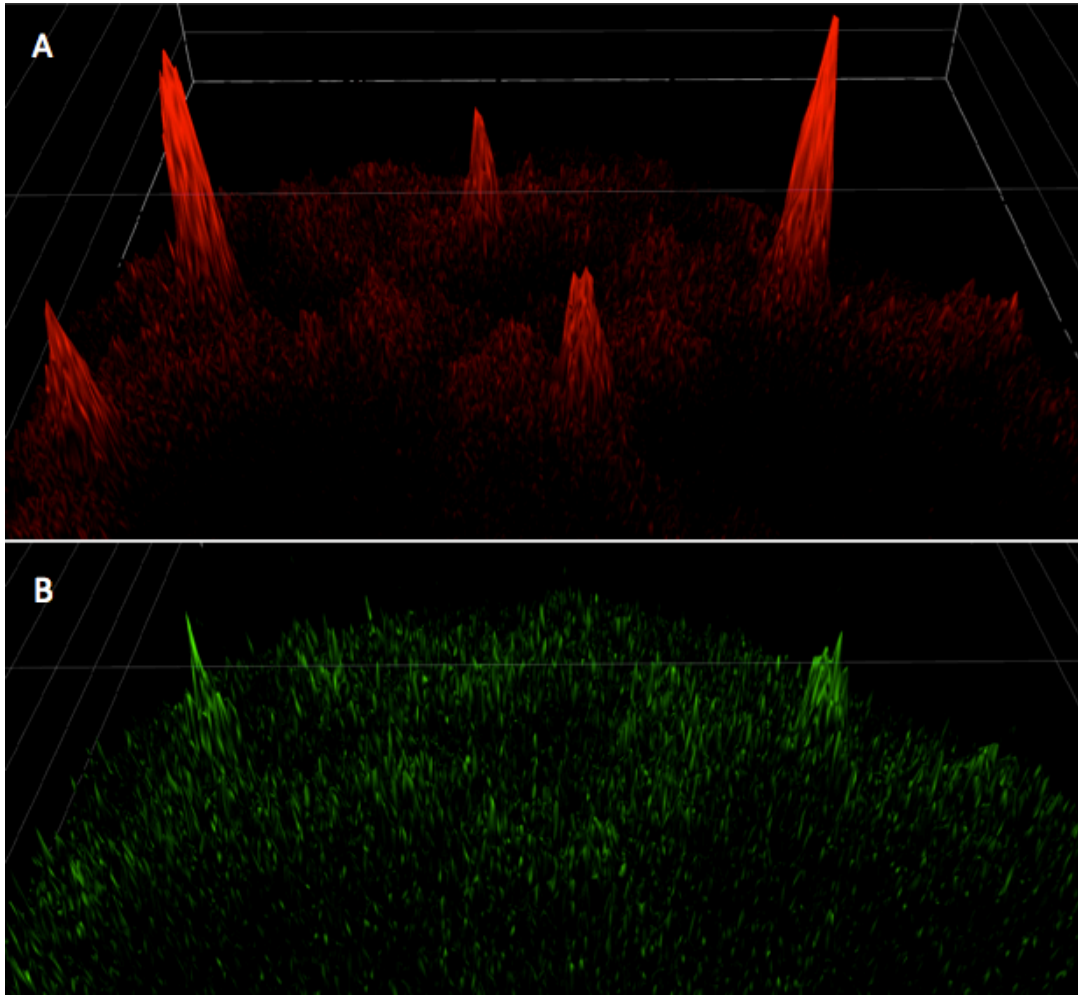


**Figure 4.5. Intensity surface plots of RBL-2H3 cell.** Intensity surface plots of z disc 10 of 26 in the red and green channels showing A) ORO and B) Fluo-4 fluorescence intensities separately. A) Five distinctive ORO peaks can be seen of varying intensities. These represent the five lipid bodies observed in Figure 4.2. B) Two distinct Fluo-4 peaks are seen in areas that are also ORO-positive. Images acquired and analyzed by NP.

In order to further investigate the peaks observed in the intensity surface plots, we cropped the original confocal z-stack to focus on each individual LB (Figure 4.6). To simplify matters, each LB was referred to using the ROI annotations in Figure 4.6.

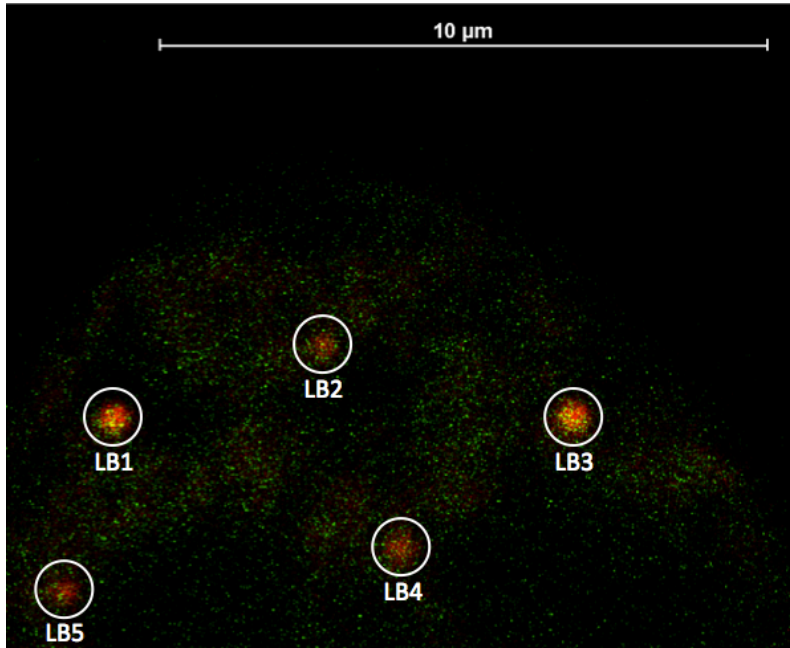


**Figure 4.6. Lipid body annotations.**

Lipid bodies (red) were named LB1 through LB5. Cropped regions were made similarly to the circle, directly around the lipid body structure. Intracellular calcium (green) can be seen throughout the cell body. Image acquired and analyzed by NP.

Once cropped, we analyzed each LB through a tiled view which displays each z-disc of the z-stack allowing for a more in-depth analysis of the entire lipid structure (Figure 4.7). The tiled view revealed several details regarding the LB. The ORO fluorescence corresponding to the LB roughly spanned 6 to 8 z-discs (0.3 micrometer thickness). We also noticed that some but not all LB also contained green fluorescence within these z-planes, mirroring the peaks we had observed on the intensity surface plots. Most striking was the placement of the Fluo-4 positive z-planes, they seemed to fall cleanly between the ORO-positive discs. While moving through images of the cell in the z-direction we observed Fluo-4 intensity appear then disappear within regions displaying ORO fluorescence, indicating that the Fluo-4 fluorescence signal is not above or below but within the LB. These observations indicated that the ORO<sup>+</sup>/Fluo-4<sup>+</sup> LB contained above background Fluo-4 positivity.

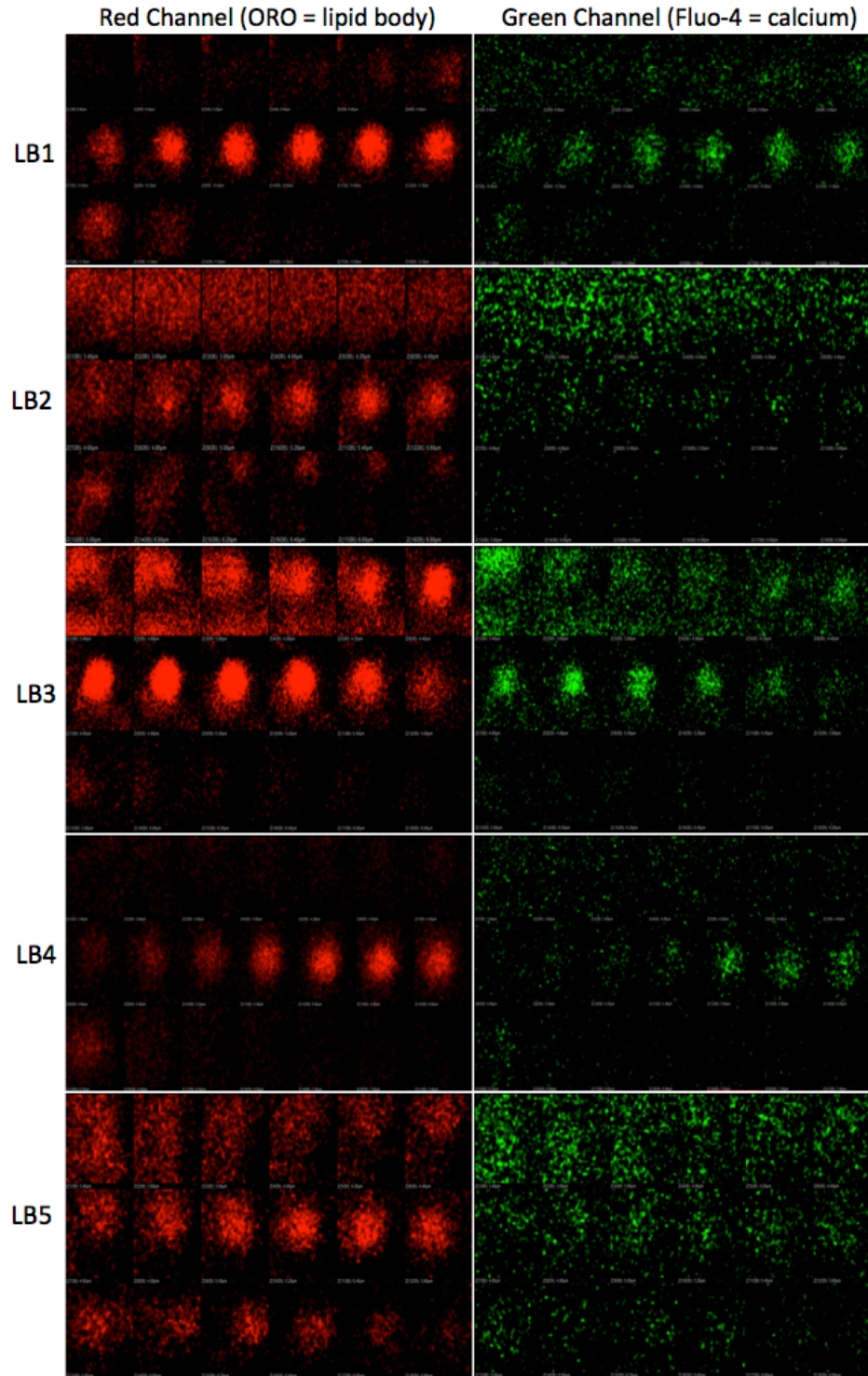


**Figure 4.7. Tiled views of lipid body z-stacks.** Z-stacks of LB1 through LB5 in the red and green channels showing the z-discs which contain the lipid body. Each tiled view contains 18 z-discs, depicting 18 discs of the 26 total discs comprising the initial z-stack. The intense red circular shapes correspond to the lipid body structure. Imaging and analysis performed by NP.

To gain a better understanding of the tiled views, analysis was performed to obtain numerical values of mean ORO and Fluo-4 intensities were calculated for each LB. A region of interest (ROI) was drawn around the LB structure. The LB was determined to be where the ORO fluorescence was most intense and is represented by ROI 1 (Figure 4.8). A second ROI, ROI 2, was drawn around the area of the LB considered to have the most calcium, indicated by increased Fluo-4 intensity.

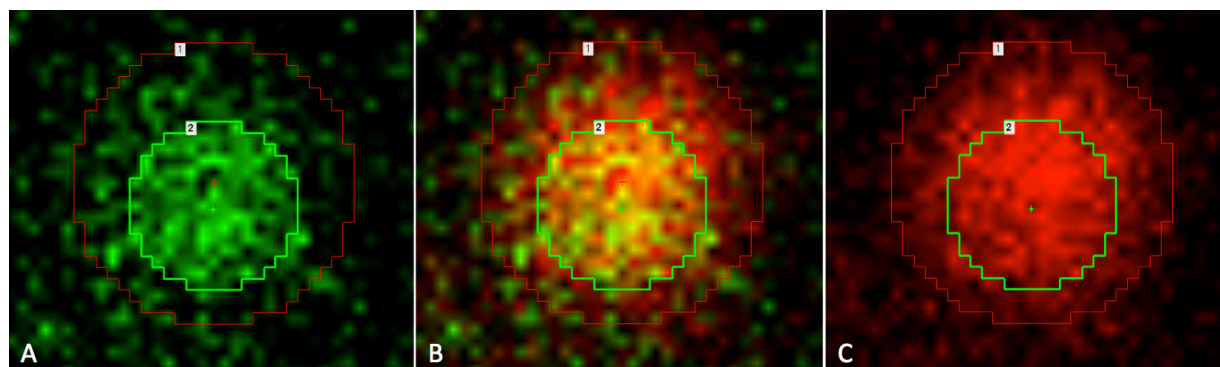


**Figure 4.8. Example of lipid body regions of interest.** A cropped z-stack of LB3 visualized in the A) green, B) red and green, and C) red channels to determine where the ORO and Fluo-4 fluorescence was most intense. Regions of interest were drawn around the lipid body and calcium-rich areas and correspond to ROI 1 and ROI 2 respectively. These ROIs were then used to measure mean fluorescence of each dye. Imaging and analysis performed by NP.

The numerical values generated through these ROIs were then plotted as a bar graph allowing for visualization of the two dyes through the entire z-stack of each LB (Figure 4.9). The graphs supported the visually-observed increases in ORO fluorescence within the LB relative to the cytosol. It also became possible to assess the extent of increased Fluo-4 fluorescence within the LB relative to the cytosol. The graph also supported the intensity surface plots (Figure 4.5) where LB1 and LB3 were the only lipids which also exhibited Fluo-4 fluorescence. LB2 and LB5 did not appear contain increased Fluo-4 fluorescence relative to the cytosol of the cell.

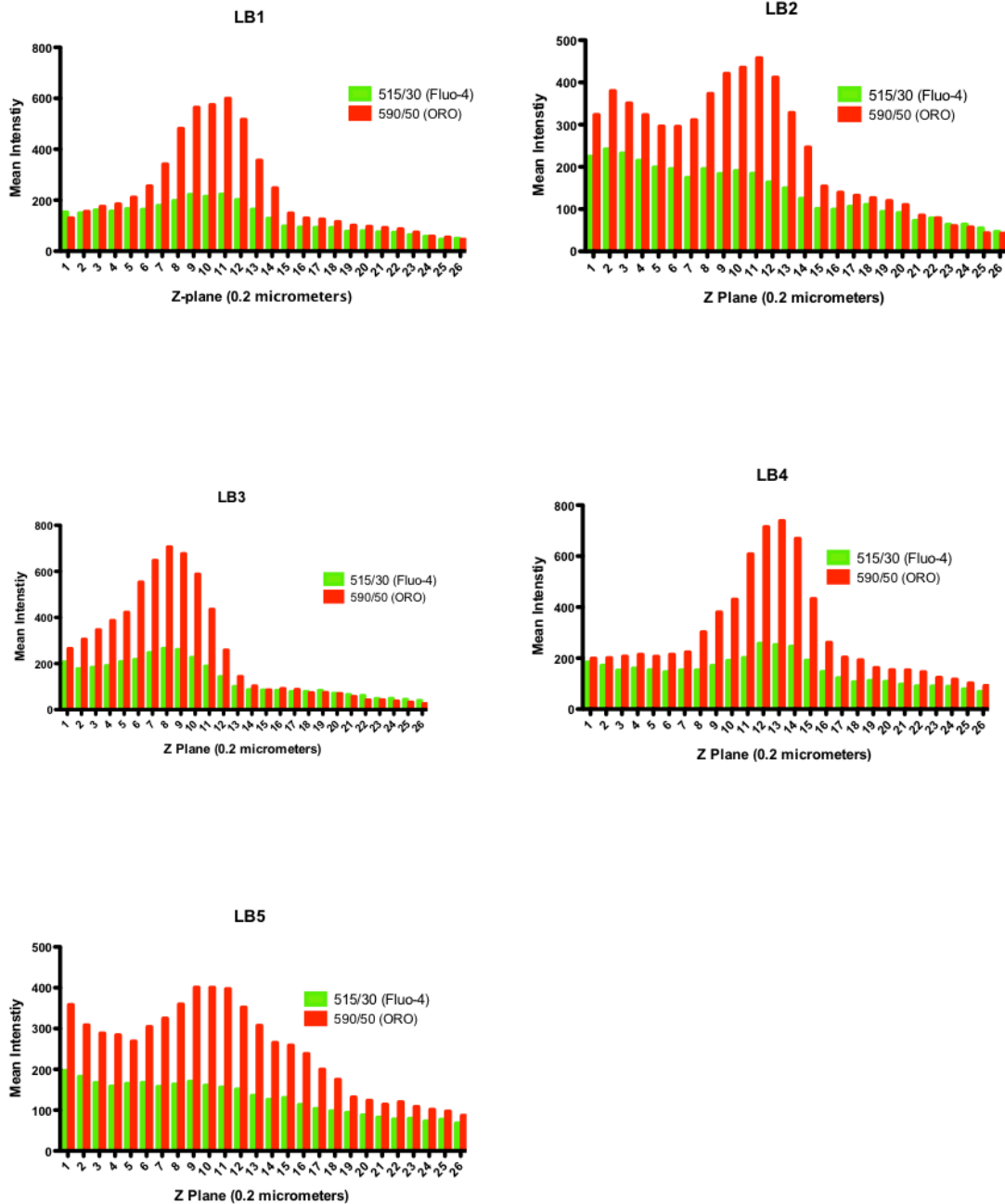


**Figure 4.9. Fluorescence intensity of ORO and Fluo-4 in lipid body z-stacks.** Mean fluorescence intensities in the red (ORO) and green (Fluo-4) channels were determined and graphed for all 26 z-discs of each lipid body. ORO mean intensity increases as the z-discs get closer to the center of the lipid body indicating an increase of ORO dye within the neutral lipid core. Fluo-4 mean fluorescence varies for each lipid body, supporting previous observations of a heterogeneous distribution of calcium throughout the cytosol. LB1, LB3, and LB4 all show an increase in mean Fluo-4 fluorescence coinciding with the intense ORO peaks, indicating an increase of Fluo-4 fluorescence within the lipid bodies. LB2 and LB5 did not appear to demonstrate an increase in Fluo-4 fluorescence relative to the cytosol. Analysis performed by NP.

In order to verify whether the LB were sequestering calcium at an above-basal cytosolic level, we performed another form of analysis. Using NIS-Elements, we drew an ROI around the LB to measure the mean Fluo-4 fluorescence intensity within the LB. An identical ROI was placed outside the LB to determine Fluo-4 fluorescence intensity of the cytosol (Figure 4.10). When placing the cytosolic ROI, the calcium concentration of the cytosol was taken into consideration. We made sure to place the ROI over a region that we thought was a good representation of the overall average cytosolic calcium levels.

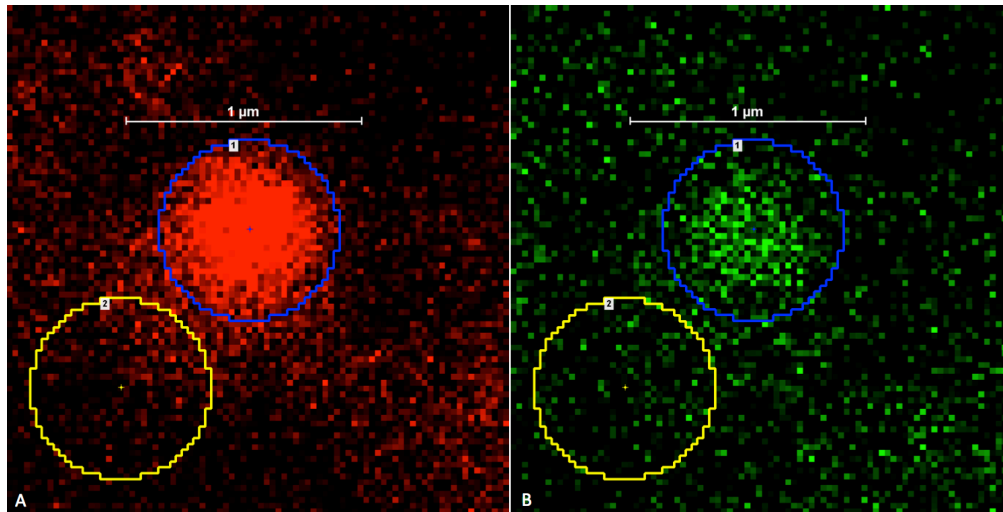


**Figure 4.10. Example of Fluo-4 fluorescence intensity comparison.** A cropped z-stack of LB3 was visualized in the A) red and B) green channels to identify the lipid and calcium respectively. Two identical ROIs are seen: ROI1 highlights the lipid body while ROI2 is placed over the cytosol. Imaging and analysis performed by NP.

Our analysis of the mean Fluo-4 fluorescence values generated within each ROI is shown in Figure 4.11. Contrasting the data shown in Figure 4.9, the average Fluo-4 intensity of the cytosol does not vary greatly over the course of analyzing the five LB. However the average Fluo-4 intensities within the LB do vary. As expected LB3 exhibited the greatest fluorescence, with LB4 slightly less, followed by LB1, LB5, and LB2. This graph demonstrated that some LB, notably LB1, LB3, and LB4 are capable of storing calcium at an above-basal cytosolic level.

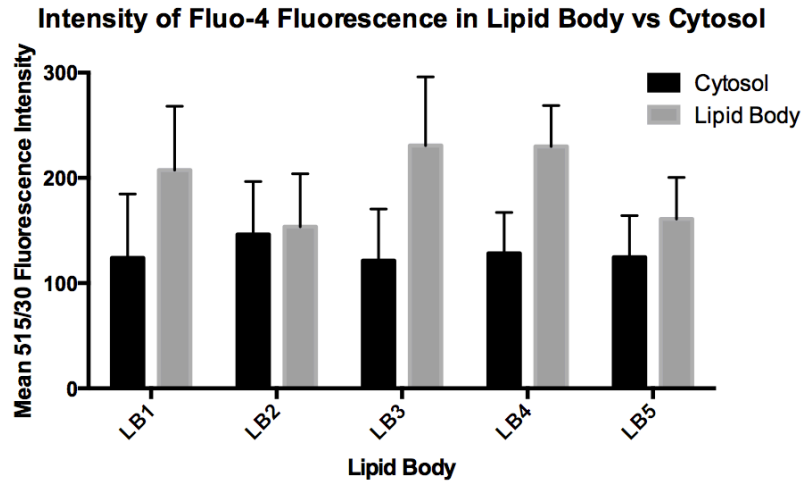


**Figure 4.11. Comparison of lipid body and cytosolic Fluo-4 fluorescence intensities.** The values generated through ROI comparison were graphed for each lipid body. Depicted are the calculated Fluo-4 intensities over the entire z-stack.

Lastly, we rendered each z-stack to produce 3-dimensional models of each LB. Figure 4.12 shows 3D renderings in the red and green channels separately and merged. All five LB are relatively spherical, with each exhibiting varying amounts of Fluo-4 fluorescence. LB1 and LB3 have the highest mean Fluo-4 fluorescence intensities which correlates to all prior analyses. Most striking was the yellow color we observed within the core of some LB. The co-location of red and green fluorescence is visualized as yellow fluorescence, indicating the simultaneous fluorescence of both ORO and Fluo-4 in those areas. These observations indicated that calcium was present within the neutral lipid core of some LB within the cell.

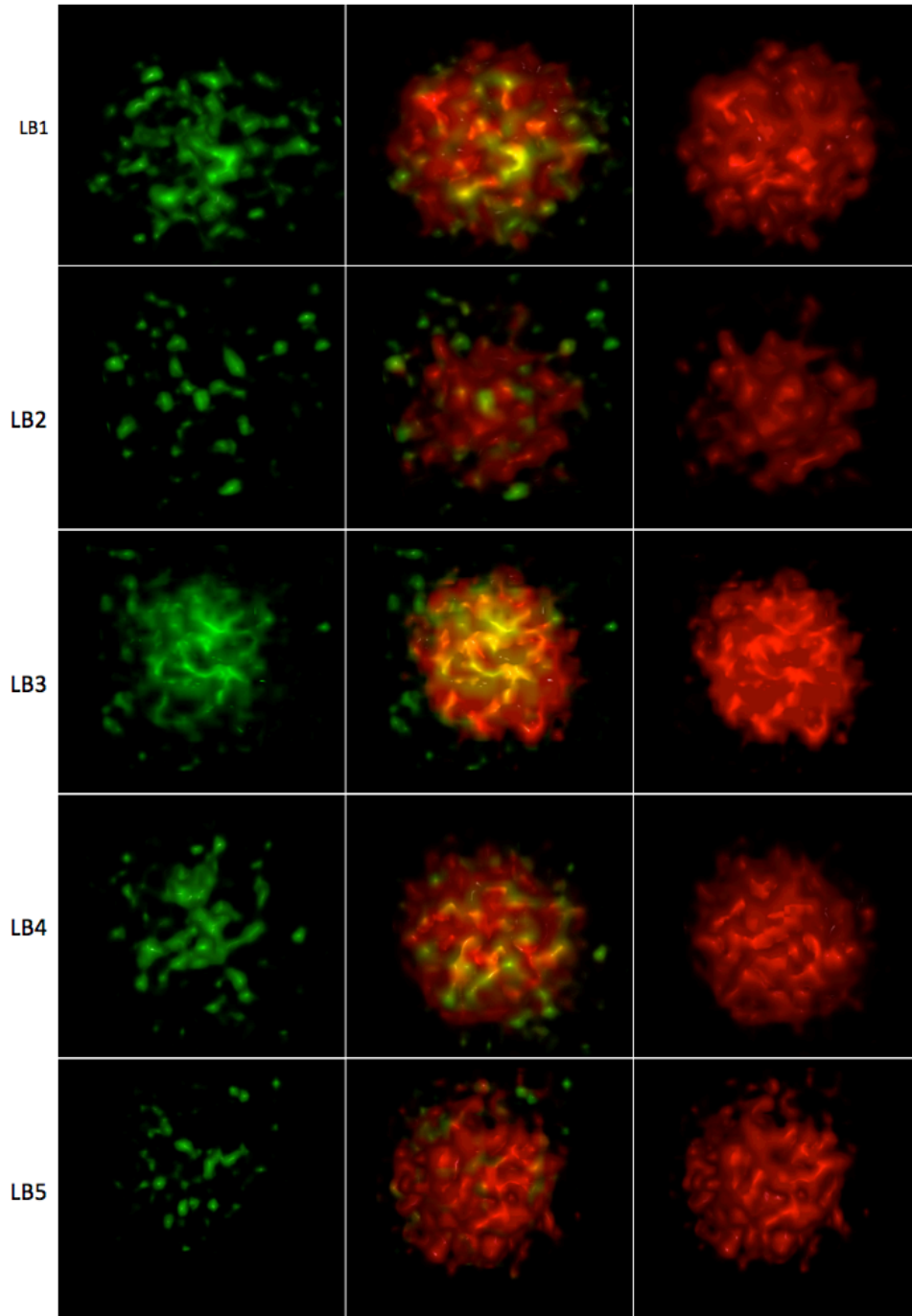


**Figure 4.12. Three-dimensional renderings of LB1 through LB5.** Volume renderings of the five RBL-2H3 lipid bodies. Left column depicts rendering in the green channel, middle column in red and green channels, with the right column showing only the red channel. The circular shape of each lipid bodies can clearly be seen with varying amounts of green (Fluo-4) fluorescence. Imaging and analysis performed by NP.

### **4.3 Discussion**

The goal of this chapter was to study the impact of an elevated LB number on mast cell calcium signaling dynamics. Through the use of ORO and Fluo-4 co-staining we observed differences in Fluo-4 fluorescence in the cytosol versus the lipid-rich areas of the cell during stimulation. Once the influx phase of the calcium response is underway, LB and the cytosol appear flooded with calcium, making it difficult to differentiate between regions of the cell that were initially ORO<sup>+</sup> and ORO<sup>-</sup>. However, once the calcium influx declined it became apparent that ORO<sup>+</sup> regions behave differently than the rest of the cytosol. Some, but not all, ORO<sup>+</sup> areas of the cell demonstrated sustained retention of high Fluo-4 fluorescence intensity. Given that ORO-positive regions correspond to LB, this would mean that LB can in fact store calcium. The sustained elevation in Fluo-4 fluorescence in ORO<sup>+</sup> LB regions may reflect them acting as long-term calcium sinks. This idea has functional and mechanistic implications. First, if LB do store calcium at above-basal cytosolic levels, then their abundance in the cytosol would be predicted to impact basal and initial calcium responses. If they act to absorb calcium from the cytosol then their increased abundance would tend to modify calcium gradients between stores and cytosol, and contribute to the reabsorption of calcium from cytosol into stores/sinks that follows depletion or influx. Second, assuming that their stored calcium can be accessed, the presence of loaded sinks after an initial stimulus would be predicted to change and shape subsequent responses to repeat stimuli. LB may variously act as sources and sinks of calcium, adding complexity to our understanding of calcium dynamics.

Using the whole-cell imaging process yielded useful results; however, the method is not without its flaws. While working with the confocal microscope a difficulty we experienced was having to choose between quality and quantity. Visualizing cells with a combination of the 100x objective and digital zoom made it possible to obtain highly detailed images of individual cells. Since these images were focused very tightly on regions containing LB, more z-discs were taken through each lipid structure. Given the small size of mast cell LB (approximately 1 micron) having more z-discs bisect the organelles resulted in a more detailed and complete analysis. However, focusing on only one cell resulted in a loss of information that could have been gained by imaging other cells in the coverslip dish. While choosing a wider field (40x or 60x objectives) would have made it possible to image more cells, this approach produced lower-quality images relative to the zoomed method. Having to choose between quality and quantity proved especially challenging when we realized that not all LB demonstrated the ability to sequester calcium. After attempting to image cells using the 60x objective, we realized that the reduced quality of the lower-powered imaging resulted in a less informative set of images for analysis. We settled on

using the highly magnified methodology of imaging, realizing that we were potentially excluding interesting LB. In an attempt to increase the number of cells viewed during imaging experiments we began pre-screening co-stained cells with the epi-fluorescence microscope. This allowed us to analyze a large number of cells and observe LB of interest via fluorescence microscopy before obtaining confocal z-stacks. In this way, we increased the likelihood of imaging LB demonstrating calcium sequestration.

## Chapter 5.

### Aim III. Is a lipid body a *bona fide* calcium store ?

#### 5.1 Introduction and goals

After observing several LB demonstrating the ability to sequester calcium, we asked whether LB are previously unrecognized calcium stores. LB are traditionally thought to mainly function as energy-storage compartments however, our observations show that they may also have the potential to store calcium. Calcium stores are capable of storing and releasing calcium in response to stimuli. If mast cell LB are capable of functioning as calcium stores this would mean that they may also be involved in immunocyte calcium signaling. If some LB function as calcium stores, this could potentially alter signaling dynamics of steatotic mast cells. The goal of this chapter is to explore our hypothesis that some LB have the potential to function as calcium stores.

##### 5.1.1. Intracellular calcium storing organelles

Mitochondria, endosomes, Golgi vesicles, and the endoplasmic reticulum are among several intracellular organelles which demonstrate the ability to store and release calcium under varying conditions (50). Of all the organelles, this accumulation and release of calcium has been most studied in the endoplasmic reticulum. The ER contains SERCA pumps which push calcium into the ER from the cytosol while the ryanodine (RYR) and inositol-(1,4,5)-trisphosphate receptor (IP<sub>3</sub>R) channels allow for the efflux of calcium from the ER into the cytosol. Due to its ability to both release and store calcium, the ER is considered a *bona fide* calcium store. A *bona fide* calcium store, is defined as an organelle which contains the pumps and channels required for the influx and efflux of calcium in response to stimuli.

##### 5.1.2. Calcium store stimulation

Release of calcium from calcium stores occurs in response to both physiological and pharmacological stimulation (51, 52). Physiological stimulation of intracellular calcium stores occurs via the crosslinking of FcεRI with IgE antibody (53). Aggregation of FcεRI results in the downstream activation of phospholipase Cγ1 (PLCγ1). Upon activation, PLCγ1 initiates the breakdown of membrane phospholipids into IP<sub>3</sub> and diacylglycerol secondary messengers. IP<sub>3</sub> can then bind and open IP<sub>3</sub> calcium channel receptors on the surface of calcium stores resulting in calcium depletion. This depletion of calcium then triggers the opening of store-operated

calcium channels located in the plasma membrane which results in an influx of extracellular calcium replenishing the depleted store.

Pharmacological stimulation of calcium stores has been achieved with the use of Thapsigargin. Thapsigargin is a plant-derived, tumor-promoting sesquiterpene lactone (54, 55) that inhibits the sarcoplasmic and endoplasmic reticulum calcium ATPase pumps. Treatment with Thapsigargin blocks the SERCA pumps, preventing the entry of calcium into the store after depletion via the IP<sub>3</sub>R and RYR channels. Physiology associated with Thapsigargin treatment includes a rapid increase in cytosolic free calcium concentrations resulting from the discharge of intracellular calcium stores. This rapid increase of calcium into the cytosol is thought to be linked to the store-operated calcium channels situated in the cell membrane which open and activate in response to internal calcium store depletion. To evaluate whether LB are *bona fide* calcium stores, we chose to treat individual LB with Thapsigargin in order to observe subsequent calcium fluxes. Given that LB are thought to originate from the ER, the unilamellar phosphatidylcholine outer layer of the lipids may contain the SERCA pumps and IP<sub>3</sub>R channels found on the endoplasmic reticulum. Should LB contain these pumps and channels they could have the potential to move calcium in response to stimuli in a similar fashion to the ER. Through the use of co-staining techniques, we will be able to observe whether the Fluo-4 fluorescence intensity within LB decreases in response to pharmacological treatment with Thapsigargin. Changes in fluorescence intensity may provide insight into the ability of LB to function as calcium stores.

## **5.2 Results**

### **5.2.1. Mast cell lipid bodies display altered calcium levels during whole cell stimulation**

We examined the Fluo-4 fluorescence over time in regions of interest selected to characterize the calcium flux dynamics of normal cytosol, pre-existing calcium stores and the LB themselves (Figure 5.1). The graphs in Figure 5.1B represent 25 ROI (1 micron in diameter) that were placed over structures defined as follows: pre-existing stores (upper panel) were vesicular structures having baseline Fluo-4 intensity at least 5 fold elevated over the bulk cytosol; cytosol (middle panel) was defined as extra-nuclear ROI with a starting Fluo-4 intensity less than 50% of the whole cell starting average intensity; LB (lower panel) were defined as ORO<sup>+</sup> structures. An example of these different ROIs is depicted in Figure 5.1A. Across a 35 second time course following antigen stimulation, the ROI averages demonstrated depletion and partial refilling of pre-existing stores. The ROI averages for the cytosol displayed slight elevations coinciding with store depletion followed by large increases in Fluo-4 intensity when store-operated influx

occurred in response to intracellular store depletion. LB ORO<sup>+</sup> areas, averaged across 25 ROI, display a complex profile of net depletion, followed by refilling and a second phase of depletion. During the influx phase these structures tend to reach a sustained high level of Fluo-4 intensity. Taken together these data indicate that LB do have a pattern of calcium response that is regulated by antigen receptor signaling pathways which differs from the responses seen in the bulk cytosol or conventional stores. However, we noted that each individual LB response was highly variable, creating a need to widen the analyses beyond the ROI-based approach.

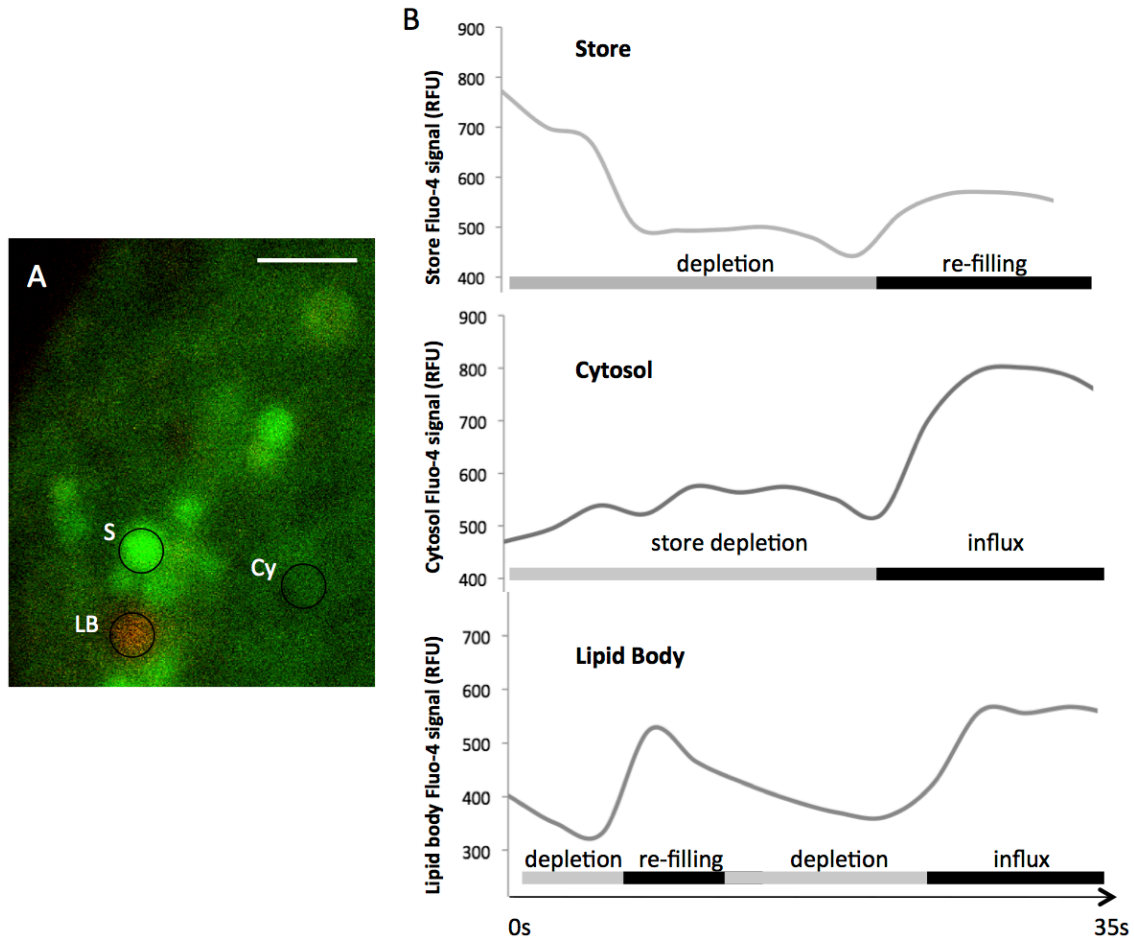


**Figure 5.1. Mean Fluo-4 fluorescence intensity of RBL-2H3** A) Zoomed in section of RBL-2H3 cell stained with ORO (red) and Fluo-4 (green). ROIs (1 micron in diameter) are drawn around a lipid body (LB), apparent calcium store (S), and cytosol (Cy). B) The mean Fluo-4 fluorescence intensity of each ROI over a time course of 35 second after stimulation with FcεRI cross-linking. Each region of the cell depicts a different Fluo-4 intensity pattern indicating the differing calcium flows throughout the mast cell. Imaging and analysis done prior to my joining the Turner lab by Helen Turner.

### 5.2.2. Assessment of isolated mast cell lipid bodies for dynamic calcium storage

The data above were generated prior to my joining the laboratory. The data suggests that in a whole cell, live cell context, LB can accumulate and disperse stored calcium in a controlled manner. At this point the next step, and where I joined the project, was to assess whether this accumulation and release activity could be demonstrated for isolated LB. This would be seen as a quite definitive test that the ability to act as a bona fide calcium store is intrinsic to the LB. Therefore the goal of the next experiment was to isolate LB by microaspiration from cells co-stained with Fluo-4 and ORO, dispense them into a calcium-containing Ringer's buffer, acquire baseline Fluo-4 images using confocal microscopy and then stimulate the LB ex vitro with Thapsigargin (Figure 5.2).

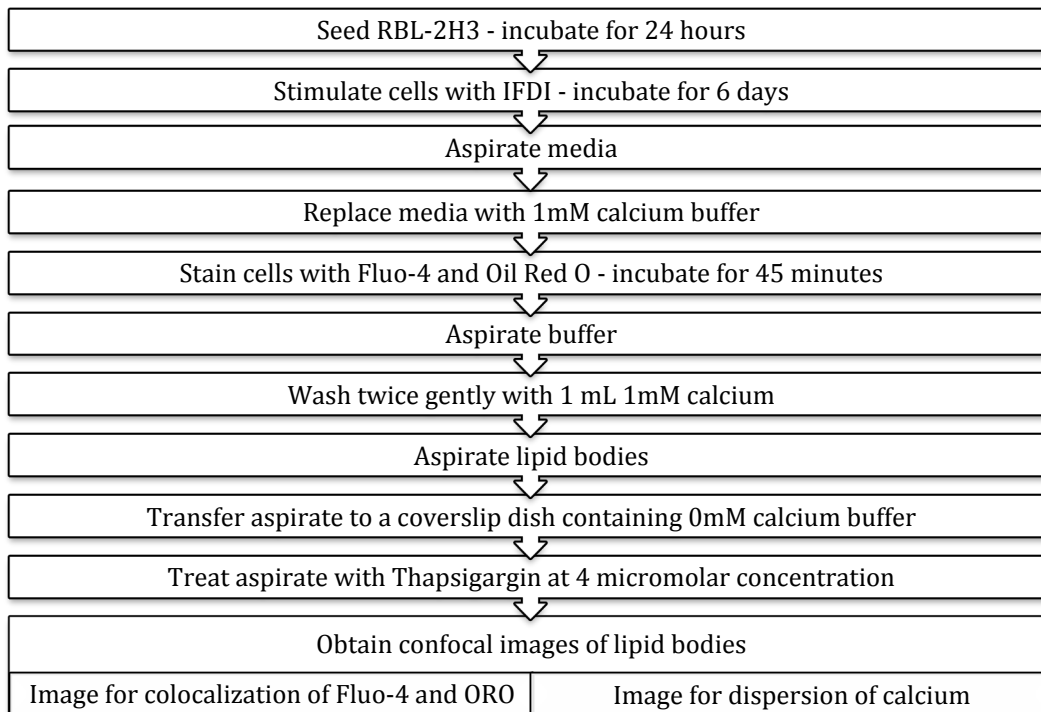


**Figure 5.2. Schematic of calcium stimulation in ex vitro lipid body manipulation.**

Once the LB aspirate from six RBL-2H3 cells was transferred to a new MatTek coverslip dish containing 1 mL of 0mM calcium buffer, we began imaging. Before obtaining confocal images of the aspirate, we first used the epi-fluorescence microscope to verify that we had successfully aspirated LB. The images we obtained through fluorescence and bright field illumination microscopy are shown in Figure 5.3. Under bright field illumination we observed a large amount

of floating LB moving quickly through the field of view. We then proceeded to view the aspirate under the Texas Red and FITC channels to verify the result of the ORO and Fluo-4 co-staining respectively. When imaging using the Texas Red channel, we observed a large amount of ORO<sup>+</sup> structures that could not be discerned in the bright field image (Figure 5.3C). While imaging using the FITC channel showed very small, punctate spots of Fluo-4 no fluorescence (Figure 5.3A).

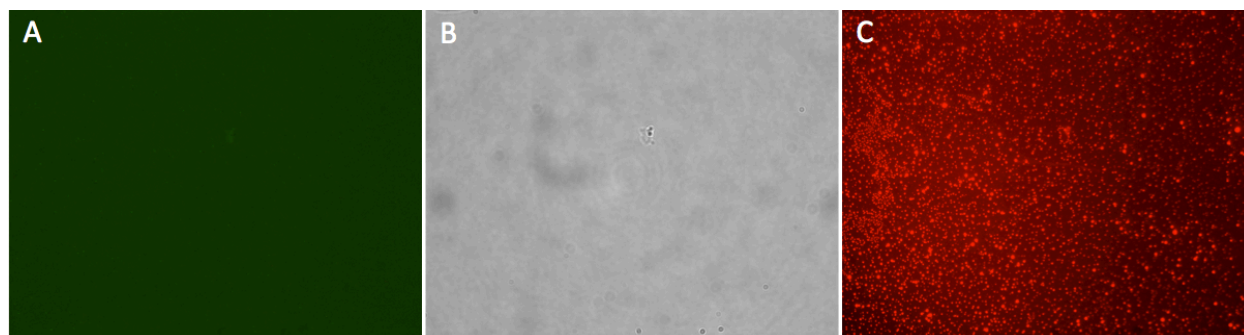


**Figure 5.3. Images of ex vivo lipid body live-staining.** Following microaspiration of ORO and Fluo-4 co-stained RBL-2H3 cells, the aspirate was expulsed into a MatTek coverslip dish containing 1 mL of 0mM calcium buffer. Bright field illumination and fluorescence microscopy images were taken to verify the presence of lipid bodies in the aspirate. A) Fluorescence image taken in the FITC channel showing punctate Fluo-4 fluorescence. B) Bright field illumination of the aspirate. C) Fluorescence image taken in the Texas Red channel showing an abundance of ORO<sup>+</sup> structures. Imaging performed by NP.

After observing the aspirate via fluorescence microscopy we realized that acquiring confocal images of aspirated LB would be difficult. The LB moved too quickly to acquire confocal z-stacks of the lipids. Although we could easily observe the ORO<sup>+</sup> structures, the Fluo-4 staining produced punctate staining that was difficult to view at 100X magnification. In order to view the results of Thapsigargin stimulation we would need to zoom into the lipids to properly view the calcium fluxes. However, due to the constant movement of the LB it was extremely difficult to track and image a single LB. Expulsing the aspirate into 1 mL of solution dispersed the lipids well enough to image. However, the large volume allowed the lipids to float around making imaging difficult. In order to properly image the calcium flux after Thapsigargin stimulation, it is necessary that the lipids remain stationary so confocal z-stacks could be acquired.

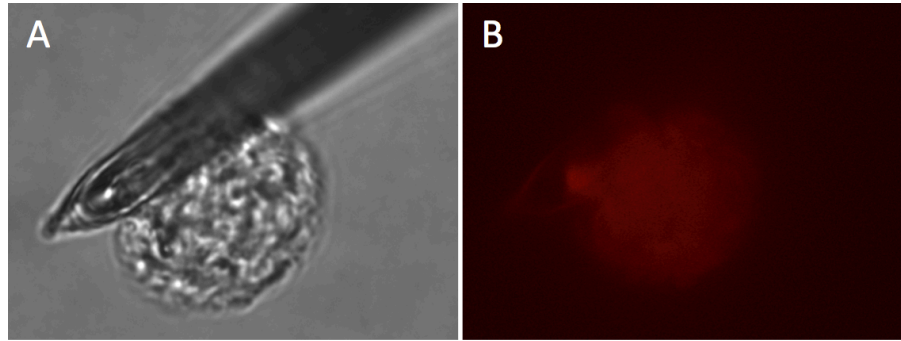


**Figure 5.4. Lipid body aspirate adhering to microinjection needle.** Expulsing the lipid body aspirate into small volumes often resulted with the aspirate clumping and adhering to the needle. A) Bright field illumination image of a ORO<sup>+</sup> lipid body clump stuck to the needle at 100X magnification. B) Fluorescence image of the same lipid clump taken in the Texas Red channel.

In an attempt to reduce LB movement, we expelled the aspirate into 10 microliter volumes. Using a smaller volume prevented floating of lipids, however the aspirate would clump and adhere to the microinjection needle in small volumes making imaging individual LB difficult (Figure 5.4).

### 5.3 Discussion

The goal of this chapter was to explore whether or not LB are *bona fide* calcium stores, containing the pumps and channels required for the store and release of intracellular calcium. Analysis of the time course experiment at the whole cell level revealed that LB demonstrate depletion and re-filling of calcium in response to IgE stimulation. This indicates that LB do exhibit a calcium response in relation to the FcεRI signaling pathway. However, our attempt to image and stimulate individual LB *ex vitro* in order to gain more insight into their calcium signaling dynamics did not yield useful results. Due to the clumping and floating of the lipids, confocal imaging could not be performed. It is possible that expelling the aspirate into a dish containing a volume between 10 microliters and 1 milliliter could present the ideal environment for even dispersion of lipids and limit floating. We could also try to reduce clumping by disrupting the cytoskeletal elements of the cell. LB have been shown to loosely associate with microfilaments and microtubules (56, 57). In a study trying to isolate LB from human eosinophils, it was demonstrated that the use of cytochalasin B and DNase I enabled the clustered LB to untangle from the cytoskeletal matrix (36). Disrupting the cytoskeletal elements associated with LB prior to aspiration and expulsion of the aspirate into a small volume could facilitate dispersion making imaging possible.

Although we were unable to observe the calcium signaling patterns of a single LB, our whole cell imaging method demonstrated that LB do exhibit the ability to store and release calcium. Various studies have proposed several ways in which LB could be acting as calcium stores. One explanation involves the association of LB with known calcium-storing organelles. Mitochondria are a specialized type of calcium store called a sink (48, 58) and have been observed in close association with LB clusters in a variety of cells (Figure 5.5) (30, 59-62). Wang et al. found that Perilipin 5 proteins (lipid storage droplet protein 5) serve as a link between mitochondria and LB. The presence of Perilipin 5 has been shown to recruit mitochondria to the surface of LB allowing for physical contact between the two organelles (61, 62). Close contact with mitochondria could confer the calcium-storing abilities that we have noticed in LB.

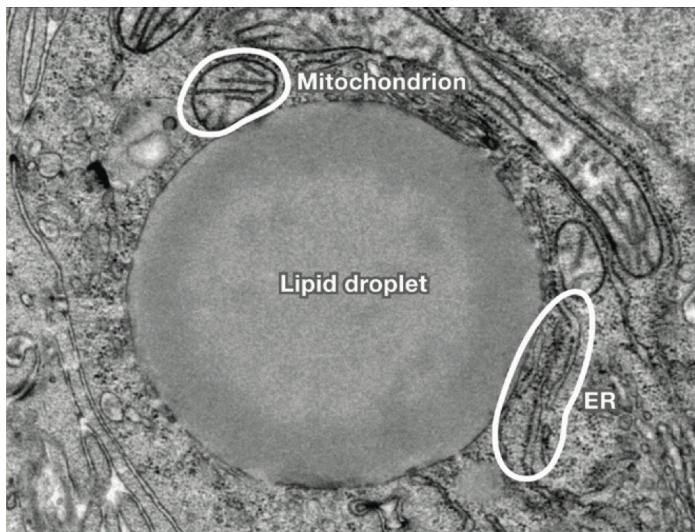


**Figure 5.5. Lipid droplet association with other organelles.** Electron micrograph of a cultured hepatoma cell depicting a lipid body, mitochondria, and endoplasmic reticulum. The unilamellar outer layer of the lipid body is closely associated with the mitochondria and endoplasmic reticulum membranes. From Farese and Walther *Cell* (2009) 139: 855-860.

During our co-staining imaging experiments we noticed LB association with Fluo-4<sup>+</sup> structures on several occasions (Figure 5.6). The LB (around 1 micron in diameter) were observed associating with one or more Fluo-4<sup>+</sup> structures (0.25 to 0.5 micro in diameter). Mitochondria, Golgi vesicles, and peroxisomes are all calcium-storing organelles which have been observed in association with LB. Although our use of Fluo-4 dye allows us to identify calcium-rich structures, we are unable to identify the organelles observed in Figure 5.6. However, sizes for each of the aforementioned calcium storing organelles have been reported to be as small as 0.5 for both mitochondria and peroxisomes making these possible identities for the Fluo-4<sup>+</sup> structures observed.

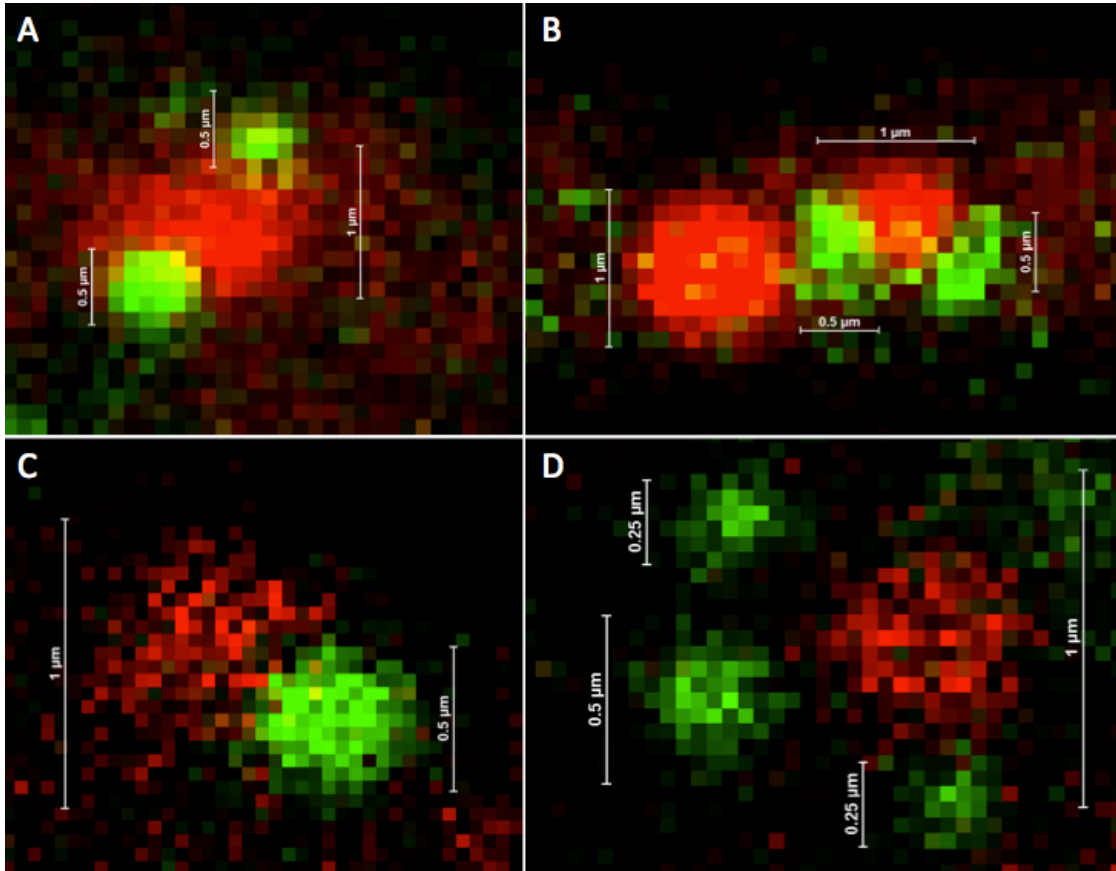


**Figure 5.6. Examples of ORO<sup>+</sup> lipid bodies in association with Fluo-4<sup>+</sup> structures.** Zoomed in confocal imaging of co-stained RBL-2H3 cells showed ORO<sup>+</sup> lipid bodies in close contact with several Fluo-4<sup>+</sup> structures. Scale bars show that lipid bodies are around 1 micron in diameter while the calcium-rich organelles averaged 0.5 microns with a few measured as small as 0.25 microns. Imaging and analysis performed by NP.

Another explanation for the apparent calcium sequestering-abilities of LB stems back to LB biogenesis. LB are thought to originate from the endoplasmic reticulum as a result of neutral lipid accumulation within the ER leaflets. Once enough lipid accumulates between the leaflets, the LB buds off taking the ER phosphatidylcholine with it to form its outer layer. Ultrastructural imaging has revealed that LB associate with ER cisternae (Figure 5.5) and that their membrane structure may be more complex than originally reported (Figure 5.7) (31). The ER is a well understood *bona fide* calcium store which has calcium pumps and channels located in its membrane. If some LB acquire more than a unilamellar layer of phosphatidylcholine from the ER, they may also be acquiring the ER's various pumps and channels. The presence of SERCA

pumps, IP<sub>3</sub>R, and RYR channels within LB would explain the calcium signaling dynamics we observed.

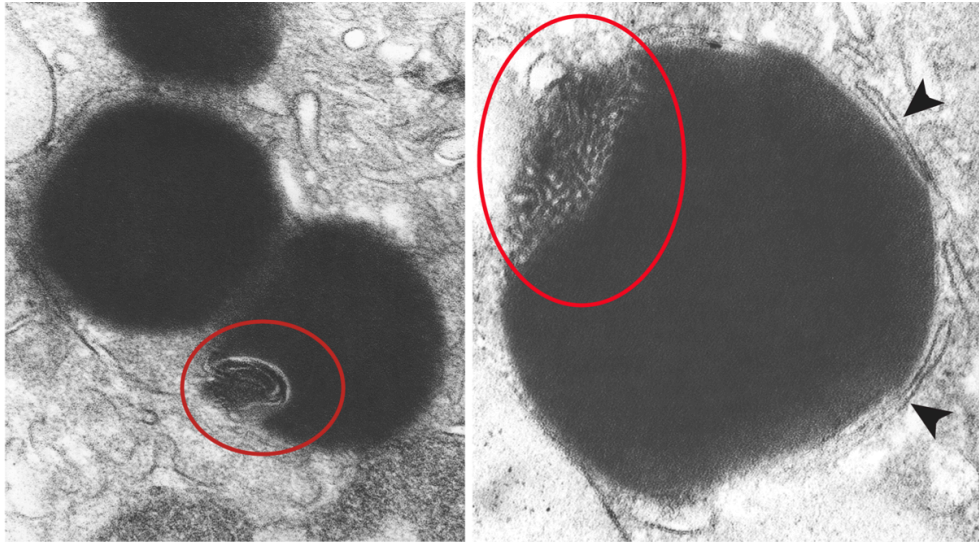


**Figure 5.7. Ultrastructural imaging of lipid bodies.** Transmission electron microscopy reveals the close association between ER cisternae (black arrows) and lipid bodies. The red circles highlight previously unreported complexities in the lipid body membrane. Distinct folds can be seen demonstrating that lipid body structure is more complex than previously reported. From Melo et al. *Plos ONE* (2013) 8(3): e59578.

LB could also be functioning as calcium stores as a result of their lipid nature. The neutral lipid core of a LB is highly viscous relative to the aqueous phase of the cytosol. During a calcium signaling event, the transcytoplasmic flow of calcium ions could be impeded or slowed by the viscosity of the LB environment leading to a passive accumulation of calcium ions. Since Fluo-4 fluoresces when in contact with calcium, our co-staining technique could be falsely giving LB the appearance of being *bona fide* calcium stores. The passive accumulation of calcium within the LB resulting from impeded flow would result in an increase in Fluo-4 fluorescence intensity due to the increased amount of calcium ions within the lipid core relative to the cytosol. The observed subsequent efflux of calcium from the lipids could then be the result of calcium ions finally traversing the LB and continuing along their original path. If the calcium storing capability of LB results from their heightened viscosity relative to the cytosol, then LB would not be *bona fide* calcium stores. However, their ability to passively accumulate calcium would make them specialized calcium stores known as calcium sinks. Should LB function as calcium sinks and slow the rate of transcytoplasmic calcium flow, this could potentially explain part of the sustained metabolic inflammation observed in individuals suffering from obesity or diabetes.

(Type II). The slow release of calcium ions could have the potential to affect downstream signaling pathways resulting in a sustained, low-grade inflammatory response.

## **Chapter 6.**

### **Discussion**

The concept that drives the work presented in this thesis is that metabolic perturbations and immune system physiology are linked. Although the fact that the metabolic and immune systems interact has been established, the extent of the effect these systems have on one another has not yet been fully explored. Several studies have demonstrated that imbalance between energy consumption and expenditure results in the accumulation of LB within adipocytes and hepatocytes, however the outcome of this energy imbalance had not yet been studied in immunocytes. Our laboratory has previously identified that insulin treatment caused mast cells to develop abnormal LB numbers, reaching steatotic states, but the effects of this increased lipid presence has not yet been analyzed. In this thesis, we identified that an increase in LB population has an effect on the calcium signaling dynamics of a cell. We also used various staining and microscopy techniques to observe the interaction between lipids and calcium more closely. We believe that these observations can provide more insight into the inflammatory responses and associated pathologies observed in those affected by metabolic disorders.

#### **What have we learned about lipid bodies?**

**1. Lipid bodies can be aspirated and fixed for imaging.** Our microaspiration technique allowed us to manipulate mast cell LB ex vitro. The ability to visualize the aspirate validated the use of microaspiration as a means of obtaining a highly purified LB sample. We were also able to fix and stain aspirated lipids with ORO for fluorescent and confocal microscopy which enabled us to observe LB shape and structure more closely. In vivo imaging experiments have demonstrated that LB closely associate with a number of intracellular organelles (21, 30, 31, 35, 59-63). Due to the relatively small size of a single LB it can be difficult at times to differentiate between structures via confocal and fluorescence microscopy. Being able to stain a large number of LB ex vitro for imaging has the potential to expand our knowledge and understanding of the supposed simple LB structure. Once fixed, LB can be stained with a variety of fluorescent dyes which could provide more insight into the LB core and membrane structures.

**2. Lipid bodies are not a homogenous organelle.** Our ORO and Fluo-4 co-staining experiments revealed that LB within a single cell are not identical. Surface intensity plots of ORO-stained cells showed that ORO fluorescence intensity is not consistent between LB. Some exhibit a higher mean fluorescence peak indicating an increase of ORO dye accumulation within

certain LB. After numerous co-staining experiments we saw that only a small percentage of the LB population contain calcium indicated by increased Fluo-4 fluorescence intensity in ORO<sup>+</sup> regions of the cell. These observations raise several questions regarding LB heterogeneity. Why do LB exhibit varying ORO fluorescence intensities? Given that ORO accumulates within the LB neutral core, do the variations have to do with the size of the core, internal structure, or the structure of the unilamellar phospholipid outer layer? Is ORO the optimal dye for observing LB in vivo? There are a number of other lipid dyes used for in lipid studies such as Nile Red or LipidtoX. Could these dyes stain a more homogenous population of lipids than ORO?

**3. Lipid bodies act as calcium stores.** LB have long been associated with energy storage however, recent studies have demonstrated that their roles extend beyond fatty acid accumulation (21, 24, 25, 31, 59, 63-65). Our data highlights a previously unrecognized LB function as a calcium store. Co-staining experiments with ORO and Fluo-4 showed that some LB sequester calcium at above-basal cytosolic levels. We also demonstrated that calcium accumulates in select ORO<sup>+</sup> areas of a cell over time in response to stimuli. It is still unclear whether LB are *bona fide* calcium stores capable of storing and releasing calcium however, we have demonstrated that LB store calcium. The ability of LB to act as calcium sinks has potential physiological implications on the calcium signaling dynamics of cells. An abundance of LB within the cytosol of a steatotic cell could affect initial calcium responses. If LB serve to absorb free calcium, this could result in signal termination while also serving as a calcium source for future intracellular processes. The presence of additional intracellular calcium sources could also be implicated in the sustained, low-grade metaflammation observed in individuals suffering from metabolic disorders.

### **What have we learned about calcium signaling in steatotic mast cells?**

Calcium signaling in steatotic mast cells is greatly reduced when compared to responses observed in a control cell. Classical calcium responses are characterized by two distinct phases 1) the initial store release followed by 2) a sustained influx of calcium via store-operated channels. Both phases are altered in cells with abnormal LB numbers. While calcium concentrations in ORO<sup>+</sup> areas of the cell did not increase as much as in ORO<sup>-</sup> regions, the ORO<sup>+</sup> regions did not experience the classical decrease of calcium concentration. Fluo-4 fluorescence was sustained in ORO<sup>+</sup> structures, indicating an increase in Fluo-4 binding to intracellular free calcium. Our observations also showed that LB behave differently from established calcium stores and the cytosol during stimulation. While LB do not demonstrate identical calcium patterns to calcium stores they do exhibit increased Fluo-4 fluorescence intensity during influx and decreased intensity during efflux indicating that calcium stored within LB may be accessible.

### **What have we learned about mast cells?**

Mast cells are traditionally implicated in allergies and type IV hypersensitivity. However, due to the increase of metabolic disorders often resulting from nutrient overconsumption, there exists an increasing body of work implicating numerous immunocytes with metabolic inflammation. An sustained increase in nutrient uptake results in the creation of LB in many cell types. Steatotic mast cells present with a lipid-dense cytosol, which may impact the body in multiple ways. First, the abnormal number of LB has an effect on transcytoplasmic signal propagation which has the potential to impact a number of downstream processes. Second, LB are known sites of eicosanoid synthesis. Lipid-derived inflammatory mediators are powerful and can have a major effect on the body. Given that steatotic mast cells contain an abnormally high number of LB, it is possible that eicosanoid synthesis is occurring within all LB. If so, steatotic mast cells could potentially be secreting an increased number of prostaglandins and leukotrienes. This increase inflammatory mediator secretion could play a role in chronic metabolic inflammation.

### **Future perspectives**

In order to achieve a more complete understanding of lipid function in mast cells it will be important to obtain a proteome. Although our use of co-staining makes it possible to track calcium flows through LB we were not able to determine whether or not a LB acts as a *bona fide* calcium store. Obtaining a proteome would provide more data and insight regarding the proteins found in LB and allow for the identification of calcium pumps and channels that may be found in LB. Our analysis showed that RBL-2H3 cells contain a very small amount of LB protein, however microaspiration yield a highly purified product. Given that the use of nanospray reduces background noise and consumes less samples resulting in a smaller sample size, a combination of mass spectrometry and nanospray has the potential to produce the proteome data we need to increase our knowledge of immunocyte LB.

Our co-staining experiments demonstrated that the LB population within a cell is heterogeneous. It would be interesting to see the results of co-staining experiments using other lipophilic dyes such as Nile Red or Lipidtox. If LB are non-homogeneous, would we observe different results through the use of different lipid dyes? Using another lipid stain may prove more favorable for identifying interesting LB (i.e. calcium-sequestering LB).

## Bibliography

1. Reaven, G.M. 1993. Role of Insulin Resistance in Human Disease (Syndrome X): An Expanded Definition. *Annu Rev Med* 44:121-131.
2. Poon, V.T.W., J.L. Kuk, and C.I. Ardern. 2014. Trajectories of Metabolic Syndrome Development in Young Adults. *PloS one* 9:e111647.
3. Emanuela, F., M. Grazia, R. Marco de, L. Maria Paola, F. Giorgio, and B. Marco. 2012. Inflammation as a Link between Obesity and Metabolic Syndrome. *Journal of nutrition and metabolism* 2012:476380.
4. Monteiro, R., and I. Azevedo. 2010. Chronic inflammation in obesity and the metabolic syndrome. *Mediators of inflammation* 2010:
5. Grundy, S.M., J.I. Cleeman, S.R. Daniels, K.A. Donato, R.H. Eckel, B.A. Franklin, D.J. Gordon, R.M. Krauss, P.J. Savage, S.C. Smith, Jr., J.A. Spertus, F. Costa, A. American Heart, L. National Heart, and I. Blood. 2005. Diagnosis and management of the metabolic syndrome: an American Heart Association/National Heart, Lung, and Blood Institute Scientific Statement. *Circulation* 112:2735-2752.
6. Bhurosy, T., and R. Jeewon. 2014. Overweight and Obesity Epidemic in Developing Countries: A Problem with Diet, Physical Activity, or Socioeconomic Status? *Sci World J* 2014:964236.
7. Popkin, B.M., L.S. Adair, and S.W. Ng. 2012. Global nutrition transition and the pandemic of obesity in developing countries. *Nutrition reviews* 70:3-21.
8. Flegal, K.M., B.K. Kit, H. Orpana, and B.I. Graubard. 2013. Association of All-Cause Mortality With Overweight and Obesity Using Standard Body Mass Index Categories. *Jama* 309:71-82.
9. Kelly, T., W. Yang, C.S. Chen, K. Reynolds, and J. He. 2008. Global burden of obesity in 2005 and projections to 2030. *International journal of obesity* 32:1431-1437.
10. Hossain, P., B. Kavar, and M.E. Nahas. 2007. Obesity and Diabetes in the Developing World — A Growing Challenge. *N Engl J Med* 356:213-125.
11. Finkelstein, E.A., O.A. Khavjou, H. Thompson, J.G. Trogon, L. Pan, B. Sherry, and W. Dietz. 2012. Obesity and severe obesity forecasts through 2030. *American journal of preventive medicine* 42:563-570.
12. Lumeng, C.N., and A.R. Saltiel. 2011. Inflammatory links between obesity and metabolic disease. *The Journal of clinical investigation* 121:2111-2117.
13. Gregor, M.F., and G.S. Hotamisligil. 2011. Inflammatory mechanisms in obesity. *Annual review of immunology* 29:415-445.

14. Greenberg, A.S., and M.S. Obin. 2006. Obesity and the role of adipose tissue in inflammation and metabolism. *Am J Clin Nutr* 83:461S-465S.
15. Krotkiewski, M., P. Björntorp, L. Sjöström, and U. Smith. 1983. Impact of Obesity on Metabolism in Men and Women. *The Journal of clinical investigation* 72:1150-1162.
16. Passante, E., and N. Frankish. 2009. The RBL-2H3 cell line: its provenance and suitability as a model for the mast cell. *Inflammation research : official journal of the European Histamine Research Society ... [et al.]* 58:737-745.
17. Zhang, J., and G.P. Shi. 2012. Mast cells and metabolic syndrome. *Biochimica et biophysica acta* 1822:14-20.
18. Wang, J., and S. Guo-Ping. 2011. Mast Cell Stabilization: novel medication for obesity and diabetes. *Diabetes Metab Res Rev* 27:919-924.
19. Lessmann, E., G. Grochoway, L. Weingarten, T. Giesemann, K. Aktories, M. Leitges, G. Krystal, and M. Huber. 2006. Insulin and insulin-like growth factor-1 promote mast cell survival via activation of the phosphatidylinositol-3-kinase pathway. *Experimental hematology* 34:1532-1541.
20. Greineisen, W.E., L.M. Shimoda, K. Maaetoft-Udsen, and H. Turner. 2012. Insulin-containing lipogenic stimuli suppress mast cell degranulation potential and up-regulate lipid body biogenesis and eicosanoid secretion in a PPARgamma-independent manner. *Journal of leukocyte biology* 92:653-665.
21. Guo, Y., K.R. Cordes, R.V. Farese, Jr., and T.C. Walther. 2009. Lipid droplets at a glance. *Journal of cell science* 122:749-752.
22. Li, Z., K. Thiel, P.J. Thul, M. Beller, R.P. Kuhnlein, and M.A. Welte. 2012. Lipid droplets control the maternal histone supply of Drosophila embryos. *Current biology : CB* 22:2104-2113.
23. Wang, Z.T., N. Ullrich, S. Joo, S. Waffenschmidt, and U. Goodenough. 2009. Algal lipid bodies: stress induction, purification, and biochemical characterization in wild-type and starchless *Chlamydomonas reinhardtii*. *Eukaryotic cell* 8:1856-1868.
24. Walther, T.C., and R.V. Farese, Jr. 2012. Lipid droplets and cellular lipid metabolism. *Annual review of biochemistry* 81:687-714.
25. Dichlberger, A., P.T. Kovanen, and W.J. Schneider. 2013. Mast cells: from lipid droplets to lipid mediators. *Clinical science* 125:121-130.
26. Bickel, P.E., J.T. Tansey, and M.A. Welte. 2009. PAT proteins, an ancient family of lipid droplet proteins that regulate cellular lipid stores. *Biochimica et biophysica acta* 1791:419-440.
27. Hsieh, K., Y.K. Lee, C. Londos, B.M. Raaka, K.T. Dalen, and A.R. Kimmel. 2012. Perilipin family members preferentially sequester to either triacylglycerol-specific or cholesteryl-ester-specific intracellular lipid storage droplets. *Journal of cell science* 125:4067-4076.

28. Robenek, H., M.J. Robenek, I. Buers, S. Lorkowski, O. Hofnagel, D. Troyer, and N.J. Severs. 2005. Lipid droplets gain PAT family proteins by interaction with specialized plasma membrane domains. *The Journal of biological chemistry* 280:26330-26338.
29. Tansey, J.T., C. Sztalryd, E.M. Hlavin, A.R. Kimmel, and C. Londos. 2004. The central role of perilipin a in lipid metabolism and adipocyte lipolysis. *IUBMB life* 56:379-385.
30. Brasaemle, D.L., and N.E. Wolins. 2012. Packaging of fat: an evolving model of lipid droplet assembly and expansion. *The Journal of biological chemistry* 287:2273-2279.
31. Melo, R.C., G.F. Paganoti, A.M. Dvorak, and P.F. Weller. 2013. The internal architecture of leukocyte lipid body organelles captured by three-dimensional electron microscopy tomography. *PloS one* 8:e59578.
32. Melo, R.C., H. D'Avila, H.C. Wan, P.T. Bozza, A.M. Dvorak, and P.F. Weller. 2011. Lipid bodies in inflammatory cells: structure, function, and current imaging techniques. *The journal of histochemistry and cytochemistry : official journal of the Histochemistry Society* 59:540-556.
33. Wan, H.C., R.C. Melo, Z. Jin, A.M. Dvorak, and P.F. Weller. 2007. Roles and origins of leukocyte lipid bodies: proteomic and ultrastructural studies. *FASEB journal : official publication of the Federation of American Societies for Experimental Biology* 21:167-178.
34. Berridge, M.J., P. Lipp, and M.D. Bootman. 2000. The Versatility and Universality of Calcium Signalling. *Nature reviews. Molecular cell biology* 1:11-21.
35. Clapham, D.E. 2007. Calcium signaling. *Cell* 131:1047-1058.
36. Weller, P.F., R.A. Monahan-Early, H.F. Dvorak, and A.M. Dvorak. 1991. Cytoplasmic Lipid Bodies of Human Eosinophils. *Am J Pathol* 138:141-148.
37. Alberts, B., A. Johnson, J. Lewis, M. Raff, K. Roberts, and P. Walter. 2002. Fractionation of Cells. In *Molecular Biology of the Cell*. Garland Science, New York.
38. Servetnick, D.A., D.L. Brasaemle, J. Gruia-Gray, A.R. Kimmel, J. Wolff, and C. Londos. 1995. Perilipins Are Associated with Cholesteryl Ester Droplets in Steroidogenic Adrenal Cortical and Leydig Cells. *The Journal of biological chemistry* 270:16790-16973.
39. Yang, Y.W., and M.D. Koob. 2012. Transferring isolated mitochondria into tissue culture cells. *Nucleic acids research* 40:e148.
40. Passante, E., C. Ehrhardt, H. Sheridan, and N. Frankish. 2009. RBL-2H3 cells are an imprecise model for mast cell mediator release. *Inflammation research : official journal of the European Histamine Research Society ... [et al.]* 58:611-618.
41. Kim, H., and D.M. Lubman. 2008. Micro-Proteome Analysis Using Micro-Chromatofocusing in Intact Protein Separations. *J Chromatogr A* 1194:3-10.

42. Haimi, P. 2011. Methods and tools for mass spectrometric lipidome analysis. In Biol and Environ Sci. University of Helsinki, Helsinki. 66.
43. Brown, H.A. 2007. Lipidomics and Bioactive Lipids: Mass Spectrometry Based Lipid Analysis. Elsevier Science, 432 pp.
44. Tabouillot, T., H.S. Muddana, and P.J. Butler. 2011. Endothelial Cell Membrane Sensitivity to Shear Stress is Lipid Domain Dependent. *Cellular and molecular bioengineering* 4:169-181.
45. Espinosa, G., I. Lopez-Montero, F. Monroy, and D. Langevin. 2011. Shear rheology of lipid monolayers and insights on membrane fluidity. *Proceedings of the National Academy of Sciences of the United States of America* 108:6008-6013.
46. Yamamoto, K., and J. Ando. 2013. Endothelial cell and model membranes respond to shear stress by rapidly decreasing the order of their lipid phases. *Journal of cell science* 126:1227-1234.
47. Yang, W., X. Guo, S. Thein, F. Xu, S. Sugii, P.W. Baas, G.K. Radda, and W. Han. 2013. Regulation of adipogenesis by cytoskeleton remodelling is facilitated by acetyltransferase MEC-17-dependent acetylation of alpha-tubulin. *The Biochemical journal* 449:605-612.
48. Graier, W.F., M. Frieden, and R. Malli. 2007. Mitochondria and Ca(2+) signaling: old guests, new functions. *Pflugers Archiv : European journal of physiology* 455:375-396.
49. Pezzati, R., M. Bossi, P. Podini, J. Meldolesi, and F. Grohovaz. 1997. High-Resolution Calcium Mapping of the Endoplasmic Reticulum-Golgi-Exocytic Membrane System. *Mol Biol Cell* 8:1501-1512.
50. Rizzuto, R., and T. Pozzan. 2006. Microdomains of intracellular Ca<sup>2+</sup>: molecular determinants and functional consequences. *Physiological reviews* 86:369-408.
51. Parekh, A.B., and J.W. Putney, Jr. 2005. Store-operated calcium channels. *Physiological reviews* 85:757-810.
52. Berridge, M.J., M.D. Bootman, and H.L. Roderick. 2003. Calcium signalling: dynamics, homeostasis and remodelling. *Nature reviews. Molecular cell biology* 4:517-529.
53. Turner, H., and J. Kinet. 1999. Signalling through the high-affinity IgE receptor FcεRI. *Nature* 402:B24-B30.
54. Lytton, J., M. Westlin, and M.R. Hanley. 1991. Thapsigargin Inhibits the Sarcoplasmic or Endoplasmic Reticulum Ca-ATPase Family of Calcium Pumps. *The Journal of biological chemistry* 266:17067-17071.
55. Thastrup, O., P.J. Cullen, B.K. Drobak, M.R. Hanley, and A.P. Dawson. 1990. Thapsigargin, a tumor promoter, discharges intracellular Ca<sup>2+</sup> stores by specific inhibition of the endoplasmic reticulum Ca<sup>2+</sup>-ATPase. *Biochemistry* 87:2466-2470.

56. Kwiatkowska, M., K. Poplonska, A. Wojtczak, D. Stepinski, and J.T. Polit. 2012. Lipid body biogenesis and the role of microtubules in lipid synthesis in *Ornithogalum umbellatum* lipotubuloids. *Cell biology international* 36:455-462.
57. Bostrom, P., M. Rutberg, J. Ericsson, P. Holmdahl, L. Andersson, M.A. Frohman, J. Boren, and S.O. Olofsson. 2005. Cytosolic lipid droplets increase in size by microtubule-dependent complex formation. *Arteriosclerosis, thrombosis, and vascular biology* 25:1945-1951.
58. Andrade, F.H., C.A. McMullen, and R.E. Rumbaut. 2005. Mitochondria Are Fast Ca<sup>2+</sup> Sinks in Rat Extraocular Muscles: A Novel Regulatory Influence on Contractile Function and Metabolism. *Inves Ophthalmol Vis Sci* 46:4541-4547.
59. Farese, R.V., Jr., and T.C. Walther. 2009. Lipid droplets finally get a little R-E-S-P-E-C-T. *Cell* 139:855-860.
60. Goodman, J.M. 2008. The gregarious lipid droplet. *The Journal of biological chemistry* 283:28005-28009.
61. Thiam, A.R., R.V. Farese, Jr., and T.C. Walther. 2013. The biophysics and cell biology of lipid droplets. *Nature reviews. Molecular cell biology* 14:775-786.
62. Wang, H., U. Sreenivasan, H. Hu, A. Saladino, B.M. Polster, L.M. Lund, D.W. Gong, W.C. Stanley, and C. Sztalryd. 2011. Perilipin 5, a lipid droplet-associated protein, provides physical and metabolic linkage to mitochondria. *Journal of lipid research* 52:2159-2168.
63. Fujimoto, T., Y. Ohsaki, J. Cheng, M. Suzuki, and Y. Shinohara. 2008. Lipid droplets: a classic organelle with new outfits. *Histochemistry and cell biology* 130:263-279.
64. Greineisen, W.E., M. Speck, L.M. Shimoda, C. Sung, N. Phan, K. Maetoft-Udsen, A.J. Stokes, and H. Turner. 2014. Lipid body accumulation alters calcium signaling dynamics in immune cells. *Cell Cal* 56:169-180.
65. Walther, T.C., and R.V. Farese, Jr. 2009. The life of lipid droplets. *Biochimica et biophysica acta* 1791:459-466.